AEDC-TR-74-93

DEVELOPMENT OF AN IMPROVED PRESSURE TRANSDUCER FOR TEST CHAMBER MEASUREMENT

R. J. Kurz
TRW SYSTEMS GROUP
ONE SPACE PARK
REDONDO BEACH, CALIFORNIA 90278

October 1974

Final Report for Period June 18, 1973 — April 1, 1974

Approved for public release; distribution unlimited.

Prepared for

DIRECTORATE OF TECHNOLOGY (DY)
ARNOLD ENGINEERING DEVELOPMENT CENTER
AIR FORCE SYSTEMS COMMAND
ARNOLD AIR FORCE STATION, TENNESSEE 37389

NOTICES

When U. S. Government drawings specifications, or other data are used for any purpose other than a definitely related Government procurement operation, the Government thereby incurs no responsibility nor any obligation whatsoever, and the fact that the Government may have formulated, furnished, or in any way supplied the said drawings, specifications, or other data, is not to be regarded by implication or otherwise, or in any manner licensing the holder or any other person or corporation, or conveying any rights or permission to manufacture, use, or sell any patented invention that may in any way be related thereto.

Qualified users may obtain copies of this report from the Defense Documentation Center.

References to named commercial products in this report are not to be considered in any sense as an endorsement of the product by the United States Air Force or the Government.

APPROVAL STATEMENT

This technical report has been reviewed and is approved.

Kenneth B. Harwood

KENNETH B. HARWOOD
Captain (CF)
Research and Development
Division
Directorate of Technology

Robert O Dietz

ROBERT O. DIETZ
Director of Technology

UNCLASSIFIED

REPORT DOCUMENTATION PAGE		READ INSTRUCTIONS BEFORE COMPLETING FORM
1. REPORT NUMBER AEDC-TR-74-93	2. GOVT ACCESSION NO.	3. RECIPIENT'S CATALOG NUMBER
4. TITLE (and Subtitle) DEVELOPMENT OF AN IMPROVED PRESSURE TRANSDUCER FOR TEST CHAMBER MEASUREMENT		5. TYPE OF REPORT & PERIOD COVERED Final Report - June 18, 1973 - April 1, 1974 6. PERFORMING ORG. REPORT NUMBER
7. AUTHOR(s) R. J. Kurz		8. CONTRACT OR GRANT NUMBER(s) F40600-73-C-0010
9. PERFORMING ORGANIZATION NAME AND ADDRESS TRW Systems Group One Space Park Redondo Beach, California 90278		10. PROGRAM ELEMENT, PROJECT, TASK AREA & WORK UNIT NUMBERS Program Element 65802F
11. CONTROLLING OFFICE NAME AND ADDRESS Arnold Engineering Development Center (DYFS) Air Force Systems Command Arnold Air Force Station, Tennessee 37389		12. REPORT DATE October 1974 13. NUMBER OF PAGES 50
14. MONITORING AGENCY NAME & ADDRESS (if different from Controlling Office)		15. SECURITY CLASS. (of this report) UNCLASSIFIED 15a. DECLASSIFICATION/DOWNGRADING SCHEDULE N/A

16. DISTRIBUTION STATEMENT (of this Report)

Approved for public release; distribution unlimited.

17. DISTRIBUTION STATEMENT (of the abstract entered in Block 20, if different from Report)

18. SUPPLEMENTARY NOTES

Available in DDC

19. KEY WORDS (Continue on reverse side if necessary and identify by block number)

pressure transducers
instrumentation
disphragms
transducer performance
test chambers

20. ABSTRACT (Continue on reverse side if necessary and identify by block number)

The present work covers development and evaluation of a revised design of a pressure transducer which is a continuation of an effort to develop an improved ultra-sensitive pressure meter for test chamber measurements. Description of the revised design and performance achieved are presented along with recommendations on further design improvement.

DD FORM 1 JAN 73 1473 EDITION OF 1 NOV 65 IS OBSOLETE

UNCLASSIFIED

PREFACE

The work in this report was performed under Contract No. F40600-73-C-0010 for Arnold Engineering Development Center, Arnold Air Force Station, Tennessee, 37389, by TRW Systems Group, One Space Park, Redondo Beach, California. This report includes work performed during the contract period 18 June 1973 to 1 April 1974 under Program Element No. 65802F. Report submitted 30 June 1974.

The author acknowledges the direct support given to this project by O. O. Fiet, D. W. McMorris, and A. E. Eglitis of TRW Systems Group and the consultation, assistance, and interest provided by MKS Instruments Company, Burlington, Massachusetts.

The work was performed under the direction of Air Force Technical Manager, Maurice A. Clermont, Maj (CF), Directorate of Technology, Arnold Air Force Station, Tennessee.

The reproducibles used in the reproduction of this report were supplied by the author.

TABLE OF CONTENTS

SECTION		PAGE
I	INTRODUCTION	7
II	THEORY	9
	2.1 TRANSDUCER ANALYSIS	9
	2.1.1 Diaphragm Resonances	9
	2.1.2 Diaphragm Reflection	10
	2.1.3 Diaphragm Capacitance and Response (dC/dP)	11
	2.1.4 Diaphragm Pressure-Current Relation (dP/dI)	12
	2.2 ELECTRONICS ANALYSIS	13
	2.2.1 Closed-Loop Operation	13
	2.2.2 Sensitivity Limits	16
	2.2.2.1 Noise	16
	2.2.2.2 Drift	18
III	DESIGN	19
	3.1 TRANSDUCER DESIGN	19
	3.1.1 Diaphragm Assembly	20
	3.1.2 Electrode Assembly	22
	3.1.3 Vacuum Materials and Seals	25
	3.1.4 Outside and Inside Volume Enclosures	25
	3.1.5 Magnet Assembly	27
	3.2 ELECTRONICS DESIGN	27
	3.2.1 Design Modification Details	29
	3.2.2 Practical Loop Stabilization	30

SECTION		PAGE
IV	SYSTEM TESTS	34
	4.1 TRANSDUCER TESTS	34
	4.1.1 Frequency Response	34
	4.1.2 Deflection Sensitivity	34
	4.2 CLOSED-LOOP OPERATION TESTS	38
	4.2.1 Calibration and Pressure Range	38
	4.2.2 Zero-Shift and Hysteresis	40
	4.2.3 Response Time	42
	4.3 TEMPERATURE TESTING	43
	4.3.1 Diaphragm Resonance Frequency Change	43
	4.3.2 Capacitance Changes	43
V	CONCLUSIONS	47
	5.1 IMPROVED TRANSDUCER PERFORMANCE	47
	5.2 RECOMMENDED DESIGN IMPROVEMENTS	48
	REFERENCES	50

ILLUSTRATIONS

Number	Title	Page
1	Transducer and Preamp/Modulator Schematic Diagram	14
2	Electronic System Diagrams	15
3	Preamp/Modulator Equivalent Circuit	17
4	Partially Diassembled Transducer and Magnet Assembly	21
5	Diaphragm Assembly with Electrode Removed	23
6	Electrode Assembly	24
7	Common Inside Transducer Volume	26
8	Magnetic Field Characteristics	28
9	Diaphragm Current-Drive Circuit	31
10	Transducer Test Setup	35
11	Diaphragm Frequency Response	36
12	Transducer Deflection Sensitivity	37
13	Transducer Calibration Data	39
14	Zero-Shift Characteristics	41
15	Temperature Dependence of Diaphragm Response Frequency	44
16	Temperature Dependence of Transducer Capacitances	46

TABLES

I	Sources of Additive Pressure Drift	18
II	Diaphragm Resonance Frequencies and Deflection Sensitivities	38

I

INTRODUCTION

The work under the present contract is a continuation of previous work under Contract No. F40600-69-C-0009. The results of the initial development effort are described in the final report covering that work[1] and the TRW proposal for the present work[2]. Considerable detail about the transducer design and development is contained in these documents and will not be repeated in this report. The previous work resulted in a number of recommended modifications to the original breadboard transducer in order to improve its performance.

The performance objectives for the improved transducer were:

1) Operating pressure range: 10^{-1} to 10^{-8} torr.

2) Operating temperature range: $-268^{\circ}C$ to $+250^{\circ}C$.

3) Ambient humidity effects: minimal and adjustable.

4) Calibration stability vs temperature: stable and reversible.

5) Zero-shift: none.

6) Response time: one-tenth second or better.

Under the present contract an almost completely new transducer was designed, fabricated and tested. The electronic control system was similar in principle to that proposed, but differed in many significant details. The performance achieved with this improved transducer was as follows:

1) Operating pressure range: 6×10^{-2} to 1×10^{-5} torr demonstrated, with 10^{-1} to 10^{-6} torr believed to be the feasible limits.

2) Operating temperature range: considerable problems in the range of 20 to $80^{\circ}C$ led us to the conclusion that operation over the objective temperature range is not feasible.

3) Ambient humidity effects: minimal and adjustable.

4) Calibration stability vs temperature: excessive zero drift with temperature made determination of the calibration impossible.

5) Zero shift: zero shift as a function of absolute pressure was not completely eliminated, but was minimal and adjustable.

6) Response time: the objective of one-tenth second was achieved.

II

THEORY

2.1 TRANSDUCER ANALYSIS

An analysis can be done if it is assumed that the tensioned diaphragm is equivalent to an ideal tensioned, flexible membrane in a vacuum. The effects of air loading and/or any "set" in the diaphragm must be assumed to be describable in terms of slight changes in the effective values of the independent parameters. A resonable experimental verification of the model would then be to check the frequency distributions of the overtones relative to the fundamental.

For a given experimental diaphragm, when the diaphragm fundamental resonance has been determined, the effective tension can then be expressed in terms of the resonance frequency and the effective specific mass (mass per unit area of diaphragm).

Regardless of air loading, the latter is probably close to the actual specific mass of the diaphragm, which is known. Thus, the effective tension is determined. Experimentally, the tension is very hard to measure, so parameterization of all equations in terms of the diaphragm fundamental resonance frequency and specific mass is useful and has been done through most of this report.

2.1.1 Diaphragm Resonances

The classical solution of the partial differentiation equation for the vibration of a tensioned circular membrane in a vacuum is well known[3] and will not be duplicated here. If $j_{o,m}$ is used to denote a zero of rank "m" of the Bessel function of order "o," then the resonance frequencies are given by:

$$\omega_m = (j_{o,m}/R_o)\ (T/\sigma)^{1/2}, \qquad \text{Eq (1)}$$

where T is the diaphragm tension, R_o is the diaphragm radius, σ is the diaphragm specific mass, and $j_{o,m}$ = 2.405, 5.52, 8.654, etc. for the radially symmetric modes.

One outstanding problem in the system design is that all these modes are independent normal modes of the diaphragm and contribute capacitance changes, but the electrodes register only some kind of surface average of each mode. Modes for which m > 0 do not generate any feedback as the electrodes are azimuthally symmetric. The high-order Bessel functions have nodes at certain radii; on each side of a node the diaphragm movement is out-of-phase and therefore its effect on electrode capacity tends to average out. The effect is greater as "o" increases. It can be reduced by using a relatively small-diameter

"spot" electrode sensing the center deflection of the diaphragm more than the periphery.

2.1.2 Diaphragm Deflection

The deflection of a circular tensioned membrane is determined by considering the radial force balance; the force due to pressure on each disc-shaped region lying within the radius "r" must be balanced by the integrated peripheral component of membrane tension. In cylindrical coordinates:

$$(\pi\ r^2)\ P = 2\ \pi\ r\ (T\ \frac{dz}{dr})$$

which yields the deflection equation:

$$z(r) = (P/4T)\ (r^2 - R_o^2) \qquad \text{Eq (2)}$$

The static local membrane deflection z is thus parabolic, goes to zero at the membrane periphery "R_o", and varies as the ratio of pressure to diaphragm tension. It is nearly the instantaneous shape of the deflection profile at the first resonance; in fact, there is an intimate relation between static deflection and fundamental resonance which will be made clearer below.

At the diaphragm center (r = 0):

$$P = -(4T/R_o^2)\ z(0)$$

The above is an effective Hooke's-Law expression as can be seen by substituting from Equation (1) for fundamental resonance to eliminate T:

$$P = -\left(\frac{4}{j_{o,m}^2}\ \sigma\ \omega_m^2\right)\ z\ (0)$$

Consider an elemental area "A" near the diaphragm center. Multiplying by "A" and remembering that "σ" is the diaphragm specific mass, the above can be put in the form:

$$F = -k_{eff}\ z(0)\ ;\ k_{eff} = \left(\frac{4}{j_{o,m}^2}\ M\ \omega_m^2\right) \qquad \text{Eq (3)}$$

Note that the expression for k_{eff} is, within the approximation $(4/j_{o,m}^2) \simeq 1$, identical to that for a simple harmonic oscillator.

One could reverse the argument and derive the approximate fundamental resonance frequency by postulating that the diaphragm center satisfies the harmonic - oscillator equation:

$$M \ddot{z}(0) + k_{eff} z(0) = F_{drive},$$

or equivalently:

$$\sigma \ddot{z}(0) + \frac{k_{eff}}{A} z(0) = P_{drive}, \qquad \text{Eq (4)}$$

where $k_{eff} = (4TA/R_o^2)$ from the deflection equation, and P_{drive} is the applied force per unit area.

The dynamic equation greatly facilitates overall loop design. Ultimately the diaphragm center response must have a reasonably well-damped response time compatible with system design objectives and also with the presence of typical structural resonances in the 0 - 1 kHz range. When such resonances are below ω_o, the diaphragm and housing tend to move as a unit; when above, a signal is produced which may overload the preamplifier.

When the loop is closed, the $\underline{J} \times \underline{B}$ force produces an additional Hooke's-Law type of restoring force of the form, $P_{drive} = -(k/A)\, z(0)$, where "k" is proportional to the loop gain.

Grouping terms in the dynamic equation (4), it is clear that the resonance frequency is moved upwards, provided that the loop bandwidth is wide enough. This may keep the preamplifier from overloading on structural resonances, as the corresponding signals are then error signals; i.e., reduced by the loop gain. On the other hand, if the loop is rolled off at low frequencies it is easier to stabilize, and also the complications produced by diaphragm overtones are avoided.

2.1.3 Diaphragm Capacitance & Response (dC/dP)

The preceding equation for diaphragm deflection can be integrated to to obtain the capacitance as a function of pressure for a stationary electrode of radius R mounted concentric and parallel at a distance "a" from the diaphragm of radius R_o.

$$C = \varepsilon \int_o^R \frac{2\pi r\, dr}{(a - z)} \; ; \quad z = (P/4T)(r^2 - R_o^2) \text{ from Eq (2).}$$

$$C = \left(\frac{\varepsilon \pi R^2}{a}\right) \left[\left(\frac{1}{X}\right) \ln \left[\frac{(1 + X) - X_o}{1 - X_o}\right]\right] \qquad \text{Eq (5)}$$

where:

$$X = \frac{PR^2}{4Ta} \quad \text{and} \quad X_o = \frac{PR_o^2}{4Ta}.$$

Using Equation (1) to express T in terms of the fundamental resonance frequency, ω_o, we have:

$$X = \frac{1.45\ P}{a\ \sigma\ \omega_o^2} \cdot \left(\frac{R}{R_o}\right)^2 .$$

The above can be written in the form:

$$C = C_o\ f(P), \text{ where } C_o = \frac{\varepsilon \pi R^2}{a} .$$

The diaphragm response dC/dP is the slope of the curve at the origin, and may be obtained by differentiation.

$$dC/dP = 1/2\ C_o / \left(\frac{a\ \sigma\ \omega_o^2}{1.45}\right). \qquad \text{Eq (6)}$$

2.1.4 Diaphragm-Pressure-Current Relation (dP/dI)

If the plane of the diaphragm is the x-y plane and the y-axis is taken as the direction of the magnetic field, $\underline{B}$; the $\underline{J}$ X $\underline{B}$ force density is:

$$F_{mz} = J_x\ B_y .$$

Integrating throughout the volume of the diaphragm corresponding to a subarea "A":

$$P_{mz} = (J_x\ t)\ B_y = I/w\ B_y$$

where t and w are diaphragm thickness and width. By differentiation:

$$(dP_{mz}/dI) = (B_y/w) \text{ newton-m}^{-2}/\text{amp} .$$

Converting units, we have:

$$dP/dI = 2.96 \text{ X } 10^{-5}\ (B/w) \text{ torr/amp}, \qquad \text{Eq (7)}$$

where B is in Gauss and w is in inches.

2.2 ELECTRONICS ANALYSIS

2.2.1 Closed-Loop Operation

The schematic of the transducer and anew preamp/modulator is shown in Figure 1, including a new drive transformer T104 added in this period. The phasor diagram at the preamp input is diagrammed in an inset. Because of the bridge design, the bridge signal has the form:

$$E_s(t) = p(t) \cos \omega t$$

where p(t) is the differential pressure and ω is the reference oscillator frequency of a few kilohertz. The corresponding phasor has a modulus that can be either positive or negative, so to speak, but the locus of its tip maintains a constant angle "ε" relative to the drive voltage phasor. In practice, there may be a small variation of "ε" with pressure due to non-ideality of the bridge components.

In addition, there is an additive error voltage of arbitrary amplitude and phase, not related to pressure, which is due to some form of leakthrough in the drive transformer. On general principles, the latter may be assumed to be time and temperature dependent. The drive leakthrough signal may arbitrarily be divided into components which are inphase or in quadrature phase with respect to the signal.

The quadrature component of the drive leakthrough signal is easily seen on a scope as it is the only signal remaining when the bridge is nulled.

The inphase component is impossible to separate from the bridge signal. Rather, its existence is inferred from the presence of the quad component at null and a hypothesis that the drive leakthrough is not constrained to be in quadrature with the signal. This hypothesis seems justified in terms of reasonable mechanisms of feedthrough, e.g., stray winding capacitances of T104, etc.

The resultant of the bridge and drive leakthrough signals has a locus which is also shown. The sum of the bridge and inphase leakthrough components goes through a perfect null; however, the quad leakthrough corrups the null. Synchronous detection driven from the master oscillator can be "tuned" to the bridge signal phasor in such a way as to reject the quad leakthrough component. The inphase leakthrough component cannot be eliminated.

The overall feedback loop and controls diagram is shown in Figure 2. In order to stabilize the loop, the transfer function of each element must be known up to frequencies well above the open-loop unity-gain frequency. A basic decision must be made:

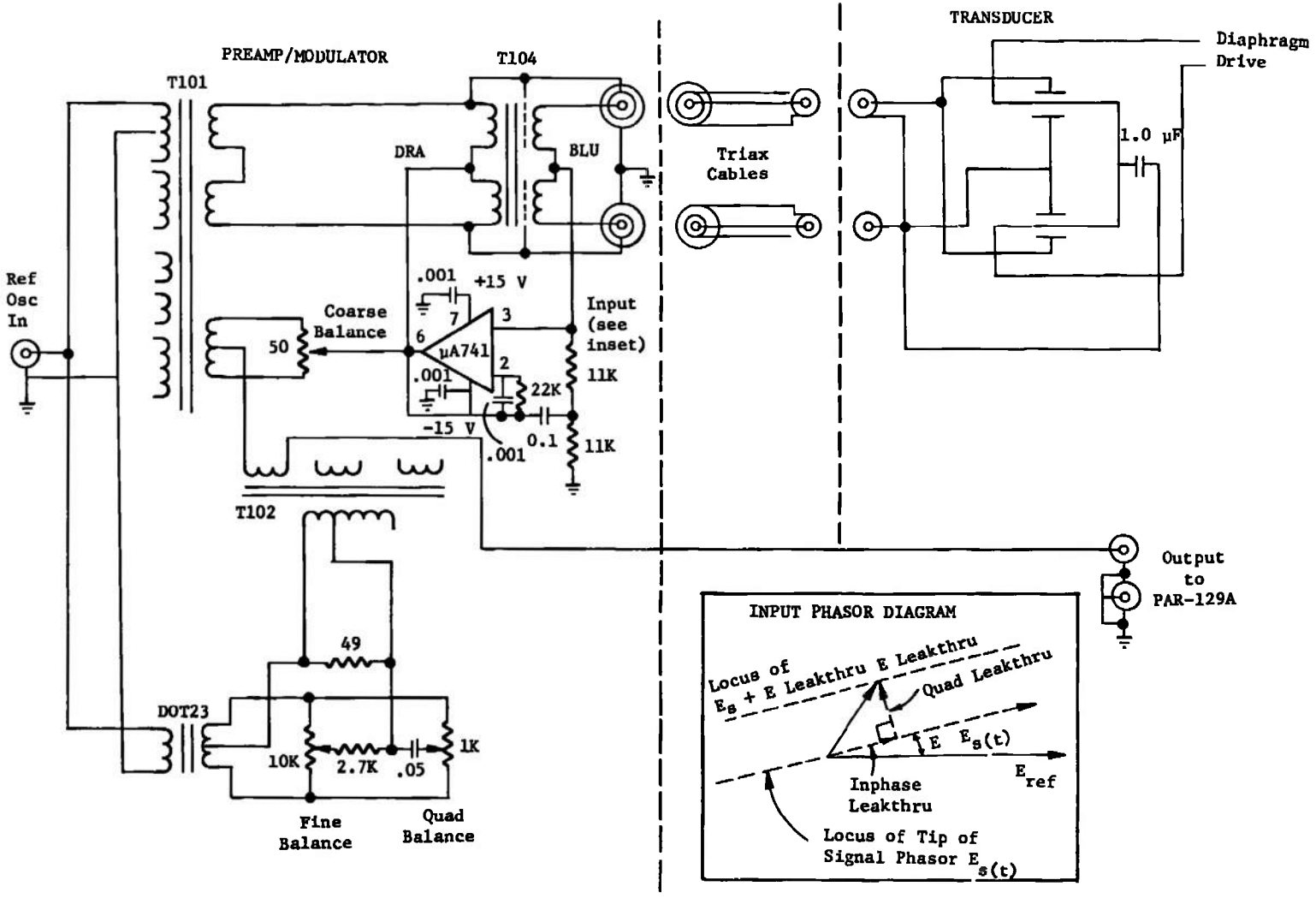

Figure 1. Transducer and Preamp/Modulator Schematic Diagram

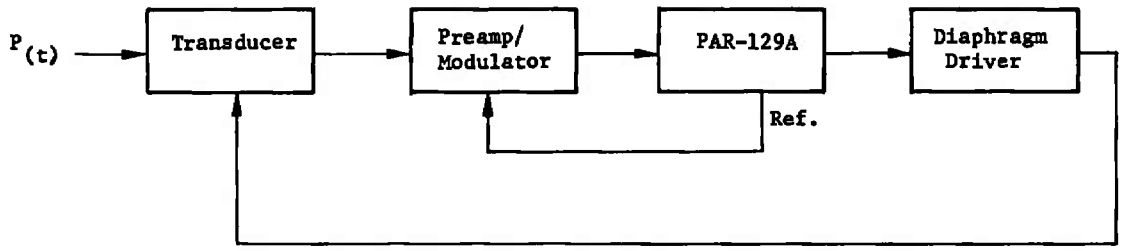

OVERALL BLOCK DIAGRAM

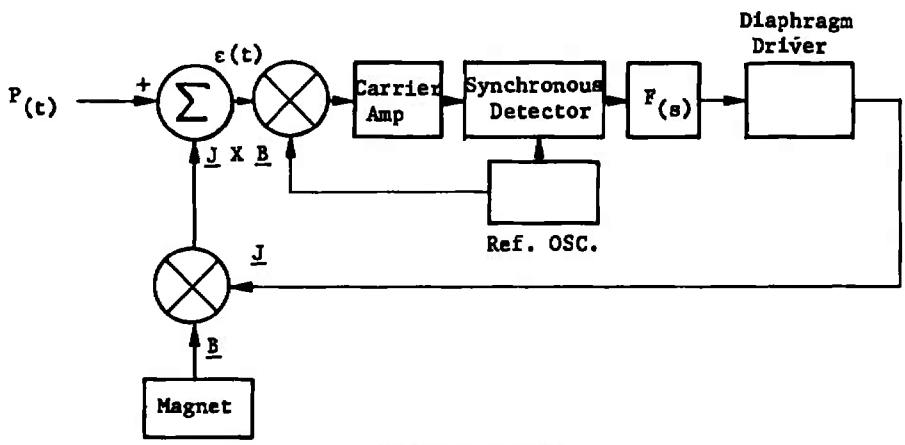

CONTROLS DIAGRAM

Figure 2. Electronic System Diagrams

1) Operate with a wideband loop encompassing the first and/or higher diaphragm resonances, or;

2) Roll off the open-loop response 6dB/octave starting from very low-frequency (op-amp type open-loop response).

In case 1) it will be seen that the resonances are in the vicinity of 500 Hz while the drive frequency is around 5kHz. The highest frequency in the pressure signal cannot exceed the drive frequency. Thus, there is a limit to the frequency range available to roll off the open-loop response. Further, the rapid phase shifts in the vicinity of the resonances are critical.

In case 2), there is a possibility of overloading the preamp with vibration-induced signals in the audio range that are uncompensated by corresponding $\underline{J} \times \underline{B}$ restoring forces because of the limited-loop frequency response.

The decision was made to design the loop to operate as in case 2), above. The primary reason for this decision was that the response characteristics of the PAR-129A lock-in amplifier used in the loop made it extremely difficult, if not impossible, to stably handle the rapid phase shifts in the vicinity of the diaphragm resonance frequency.

2.2.2 Sensitivity Limits

The factors which limit sensitivity lie within the transducer and its low-level electronics. They include transducer and preamp noise, acoustic vibration, and various drifts in the transducer and electronics.

2.2.2.1 Noise

The mid-to-high frequency equivalent circuit at the preamp input is shown in Figure 3. The various equivalent parameters include the effective parallel input resistance and capacitance of the bootstrapped op-amp circuit, the op-amp noise parameters, and the equivalent parallel losses of the transducer electrode-to-diaphragm capacitance

The theoretical op-amp noise voltage is about 10 microvolts for a 10 kHz bandwidth. The corresponding sensitivity limit is:

$$P_{min} = e_n/(dE_{in}/dP)$$

where:

$$(d\ E_{in}/dP) = (dC/dP)/(dE_{in}/dC)\ .$$

EQUIVALENT CKT

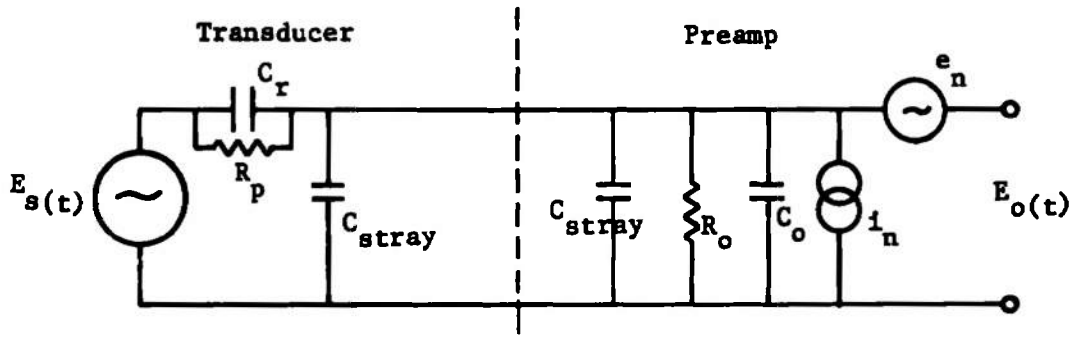

$E_{s(t)}$ = same as in Figure 1

C_T = transducer total "C" = 150 pf

$R_p = 11/j\omega c_T 1^2/R_N$ where R_N = electrode spreading res. ≃ 10 Ω

C_{stray} ≃ 15 pF

$(1/R_o + j\omega c_o) = R_{in} A_r (1 + j\omega/\omega_o)$ where R_{in} = 11K

Av and ω_o are op-amp parameters ≃ $10^6 + 2\pi \times 10^2$ respectively

e_n and i_n are op-amp noise parameters

SIMPLIFIED VERSION

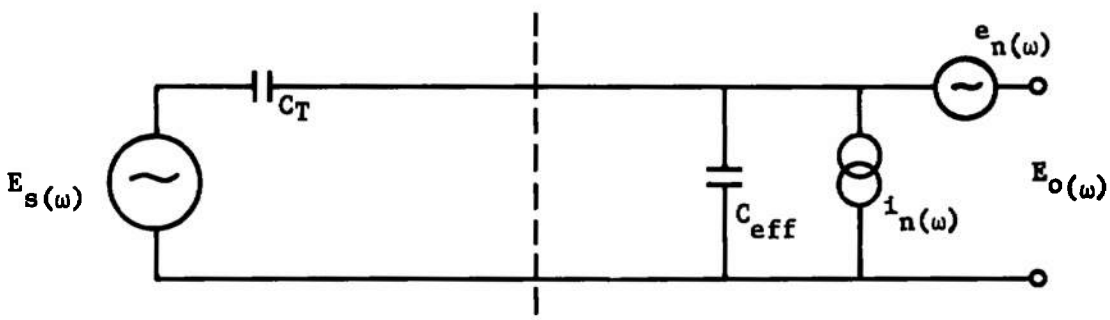

$C_{eff} = C_o + C_{strays} \simeq 20$ pF

$E_{o(\omega)} \simeq (E_{s(\omega)} + e_{n(\omega)})$ ref. oscillator frequency

Figure 3. Preamp/Modulator Equivalent Circuit

Using e_n = 10 microvolts, (dC/dP) = 100 pf - torr^{-1}, and $dE_{in}/dC = 25$ mV - pF^{-1}. P_{min} is about 10^{-6} torr.

Reducing bandwidth to 1 Hz would reduce this limit to 10^{-8} torr, in general agreement with previous estimates.

2.2.2.2 Drift

Various sources of zero drift (additive drift) are summarized in Table I. In the present program it was not possible to determine which was dominant. The experimental results on zero drift will be discussed in Section 4.2.

With a sufficiently high feedback factor, the major sources of calibration drift (multiplicative drift) are the temperature coefficient of the 0.1-ohm shunt resistor used to measure the diaphragm current, the effect of diaphragm tension variation on the loop transmission constant "Aβ" (note that $\underline{J} = \underline{J}_{ideal} \left(\frac{A\beta}{1 + A\beta}\right)$, and the temperature effect on the magnetic field. None of these effects are expected to be greater than a few percent under normal operating conditions. However, they could become significant during operation over the full objective temperature range.

TABLE I

Sources of Additive Pressure Drift

1. Temperature Effects

   1.1 Thermal expansion of housing
   1.2 Dielectric constant variation
   1.3 Temperature drift of diaphragm tension

2. Indirect Pressure Effects

   2.1 Gas composition variation
   2.2 Pressure-induced housing strain
   2.3 Pressure-induced dielectric unloading

3. Mechanical Effects

   3.1 External housing strain
   3.2 External dielectric unloading

4. Electronic Effects

   4.1 PAR - 129 equivalent input drift
   4.2 Stray capacitance drift at PAR - 129 input
   4.3 Op - amp, etc., drifts in output servo amplifier

III

DESIGN

3.1 TRANSDUCER DESIGN

On the basis of the previous development effort, a number of improvements in the transducer design were recommended. The design changes are described and the rationale for each is given in the final report[1] on the previous development work and the technical proposal[2] for the present work. The recommended changes were:

1) Change to a nonmagnetic, high-conductivity diaphragm.

2) Use frame and diaphragm materials with matching coefficients of thermal expansion.

3) Use a narrower diaphragm for increased current deflection sensitivity.

4) Minimize the use of materials that outgas and deteriorate the vacuum performance.

5) Modify the magnet pole pieces to reduce the air gap and, hence, increase the magnetic flux density in the plane of the diaphragm.

6) Scale dimensions to a smaller size while retaining the same performance characteristics.

The original intent was to incorporate most of the changes as modifications to the breadboard transducer fabricated in the previous effort. However, testing performed on the breadboard transducer in the beginning phases of the present work led us to the conclusion that attainment of the performance objectives could not be achieved with the breadboard transducer. Therefore a completely new transducer was designed and fabricated. In the course of replacing the iron diaphragms of the breadboard transducer, it was determined that it was impossible to reliably establish and hold the required tension in the diaphragms. Since the diaphragm frequency characteristics (and hence tension) are critical to the electrical performance of the closed-loop system, this feature of the breadboard transducer made complete checkout of closed-loop performance impossible. In addition, the capacitance values of the inner and outer electrodes of the breadboard transducer were quite different due to slight differences in their construction details. In the previous work, this difference was compensated by added external capacitors to balance the bridge network. However, since the external capacitance has completely different behavior as a function of temperature, humidity, absolute pressure, etc. from the actual transducer electrodes, it would be impossible to attain stable performance as these parameters varied.

The design of the improved transducer incorporates the first five of the recommended changes listed above. The transducer size was not changed significantly because the original magnets were retained. In addition to these changes, the improved transducer was also designed as a completely closed, vacuum tight system so that testing could be performed more conveniently without having to place the entire assembly in a vacuum chamber. Figure 4 is a photograph of the improved transducer in a partially disassembled state. One of the two identical sides is disassembled to show the individual elements of the complete transducer. From the left we see the outer volume cover with a vacuum flange connection and shielded electrical connection for the outer sensing electrode. Next is an electrode-diaphragm assembly that includes both the identical inner and outer electrode assemblies attached to the double-plate diaphragm frame. The current-carrying diaphragm is bonded in tension between the two plates. The common inside volume is in the center and includes vacuum connections and independent, shielded electrical connections to both of the inner electrodes. The right side of the transducer is completely assembled. The magnet assembly is at the top of the photograph. When completely assembled, the transducer is located inside the magnet assembly with the pole piece projections extending into the diaphragm assemblies.

3.1.1 Diaphragm Assembly

The diaphragm assembly forms the heart of the transducer and has the most stringent design requirements. The diaphragm must be attached to the frame in such a way that it is stably held in tension, is electrically insulated from the frame, and, finally, is vacuum sealed with a minimum amount of potential outgassing materials exposed to the working volume. These requirements are satisfied in the improved transducer by adhesively bonding the diaphragm between two flat plates in a tensioned state. The diaphragm is 0.001-inch thick tough pitch copper foil and the fram plates are OFHC copper. The match in temperature coefficients is exact so that changes in the diaphragm tension as a function of temperature are minimized. A polyimide adhesive is used to bond the diaphragm because of its good outgassing properties and stable lap shear strength as a function of temperature and age.[4]

The procedure used for bonding the diaphragm to the frame is as follows. A smooth sheet of copper foil is first bonded to a stretcher ring with the same adhesive. After curing, this foil is tensioned by placing it over a mandrel which has the shape of a truncated cone. The ring is pulled down to the periphery of the mandrel by a predetermined amount to produce the desired tension. While in this tensioned condition, one plate of the frame is bonded to the taut diaphragm with the polyimide adhesive. Once this bond is cured, the diaphragm is cut away from the ring and trimmed to the outer dimensions of the plate. Finally, the second plate is bonded to the other side of the

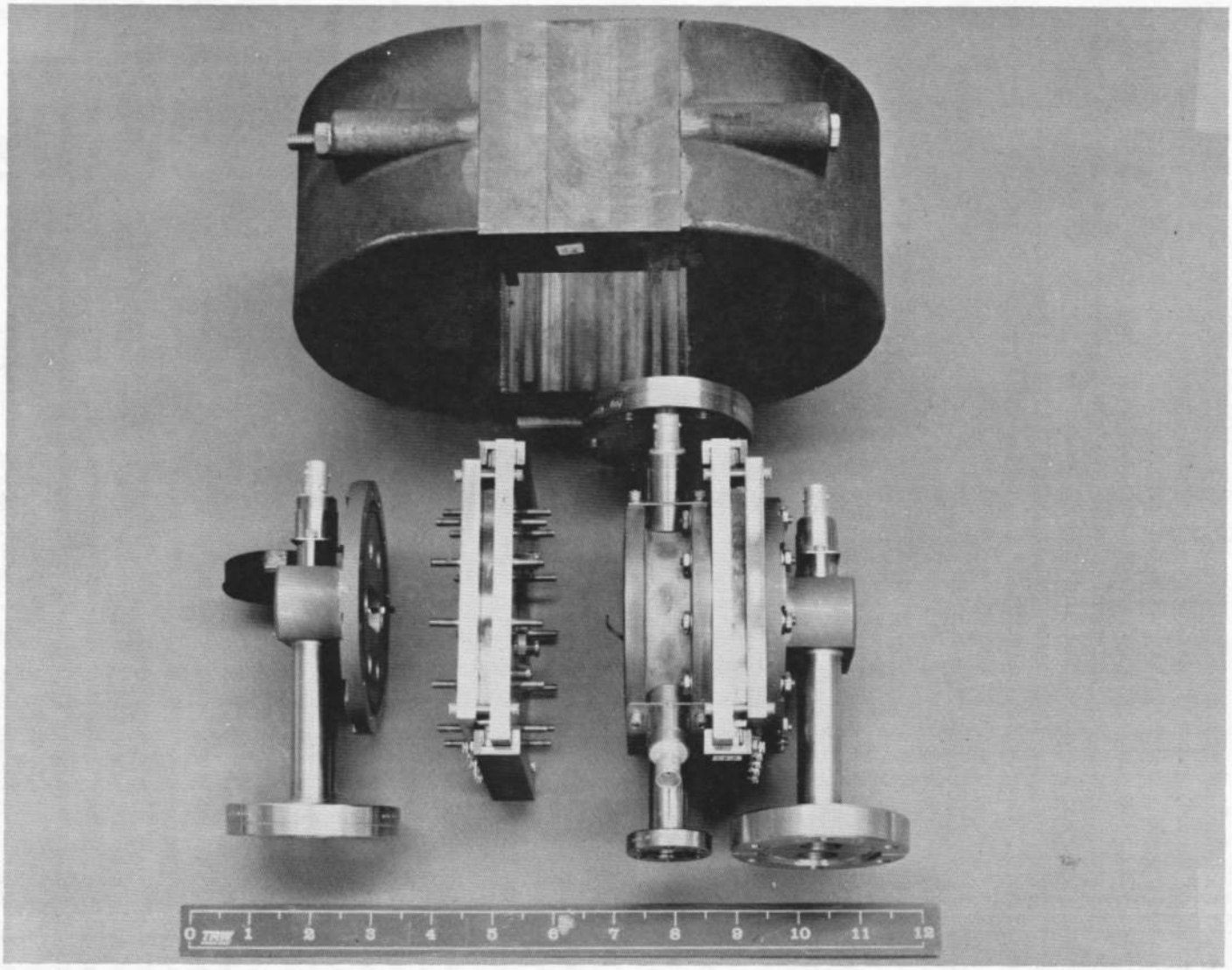

Figure 4. Partially Disassembled Transducer and Magnet Assembly

diaphragm sheet, completing the diaphragm-frame assembly. The mechanical characteristics of the diaphragm assembly were entirely satisfactory. Trouble was encountered with lack of complete electrical insulation and vacuum leaks through the adhesive. It is believed that more precise tooling for the bonding operation in order to assure uniform adhesive distribution and thickness would result in a higher yield of entirely satisfactory diaphragm assemblies than we encountered during the current work. Figure 5 is a photograph of a diaphragm assembly with the electrode assembly removed to show the diaphragm. The step around the diaphragm circumference forms the seat for the electrode assembly.

3.1.2 Electrode Assembly

The major design requirement for the electrode assembly is to obtain a high capacitance value (i.e., close spacing between the diaphragm and the electrode surface) with a minimum of stray capacitance to the frames. In addition, the capacitance of each of the electrodes must be closely matched. The electrode to diaphragm spacing in the improved transducer is 0.004 inches. A good match of the capacitances therefore requires control of the spacing to within 1/10,000 inch. It was felt that this tolerance exceeded reasonable machining tolerance and therefore a positioning mechanism was adopted to allow matching after assembly. The electrode plate is mounted to a ring, which in turn mounts rigidly to the frame with three differential screws. The screws produce a linear displacement of 0.002 inch per revolution and, hence, allow convenient and precise adjustment of the electrode diaphragm spacing. In addition to providing the ability to adjust the individual electrodes, it is important that the two electrodes be of identical design so that any changes in their capacitances due to temperature, gas composition, etc. will also be matched. In first order, it is not necessary that the capacitances each be fixed, but only that they be equal so that the bridge is balanced when the diaphragm is undeflected.

The design approach adopted to minimize stray capacitance to the frame was to form the electrode as a thin metallic film on an insulator plate with the metallic electrode diameter much less than the plate diameter. The electrode plate is fabricated of Corning machinable glass ceramic which can be easily and precisely machined.[5] In addition, the material is an excellent vacuum material with very low surface absorption. Figure 6 is a photograph of the electrode assembly viewed from the electrode side. The electrode is perforated with a large number of holes for high gas conductance. The electrode plate is 2.5 inches in diameter and the diameter of the metallic electrode is 1.5 inches. The electrode is vacuum deposited on the glass ceramic plate. First a layer of chromium is deposited for good adherence to the ceramic and then a layer of gold several

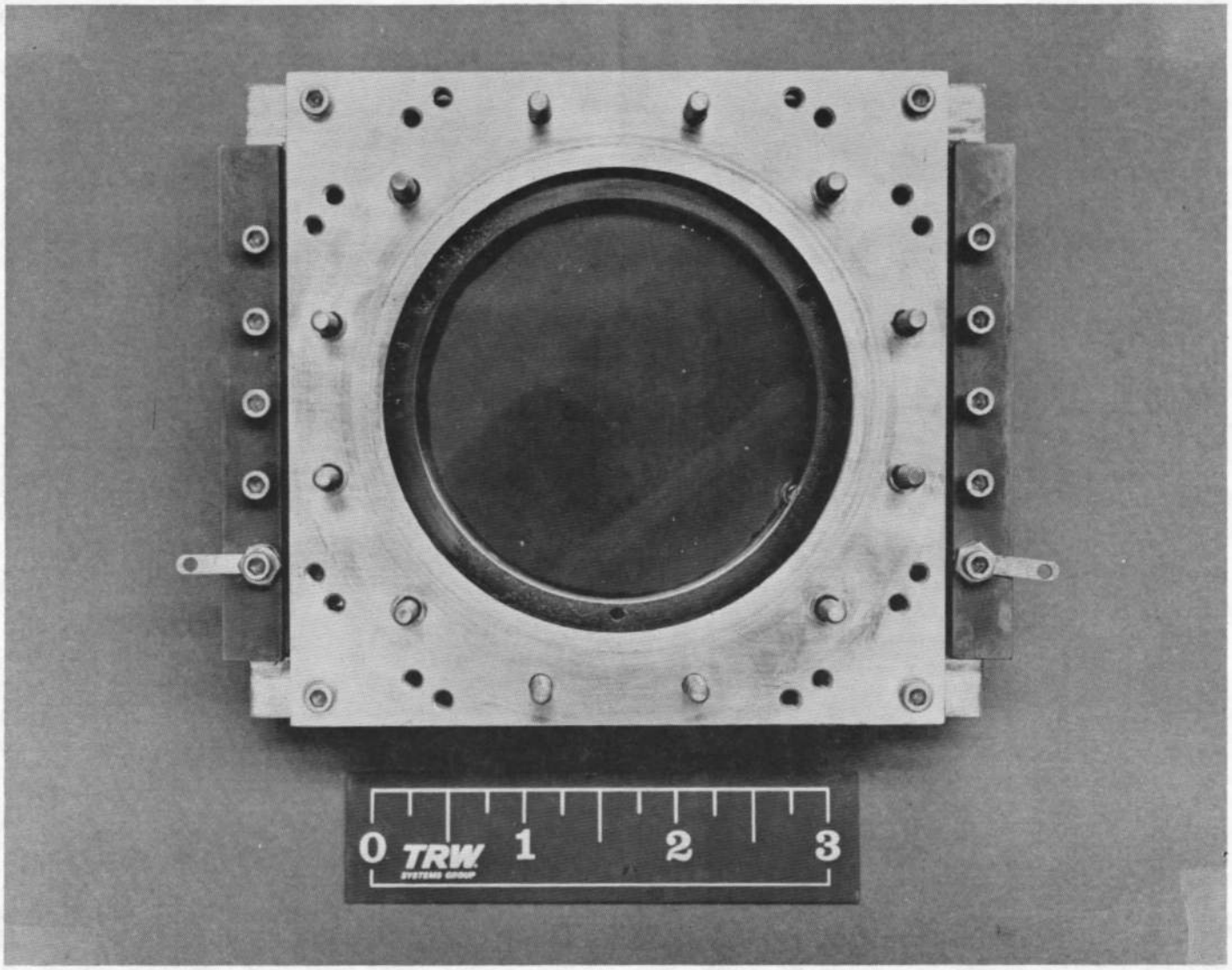

Figure 5. Diaphragm Assembly with Electrode Removed

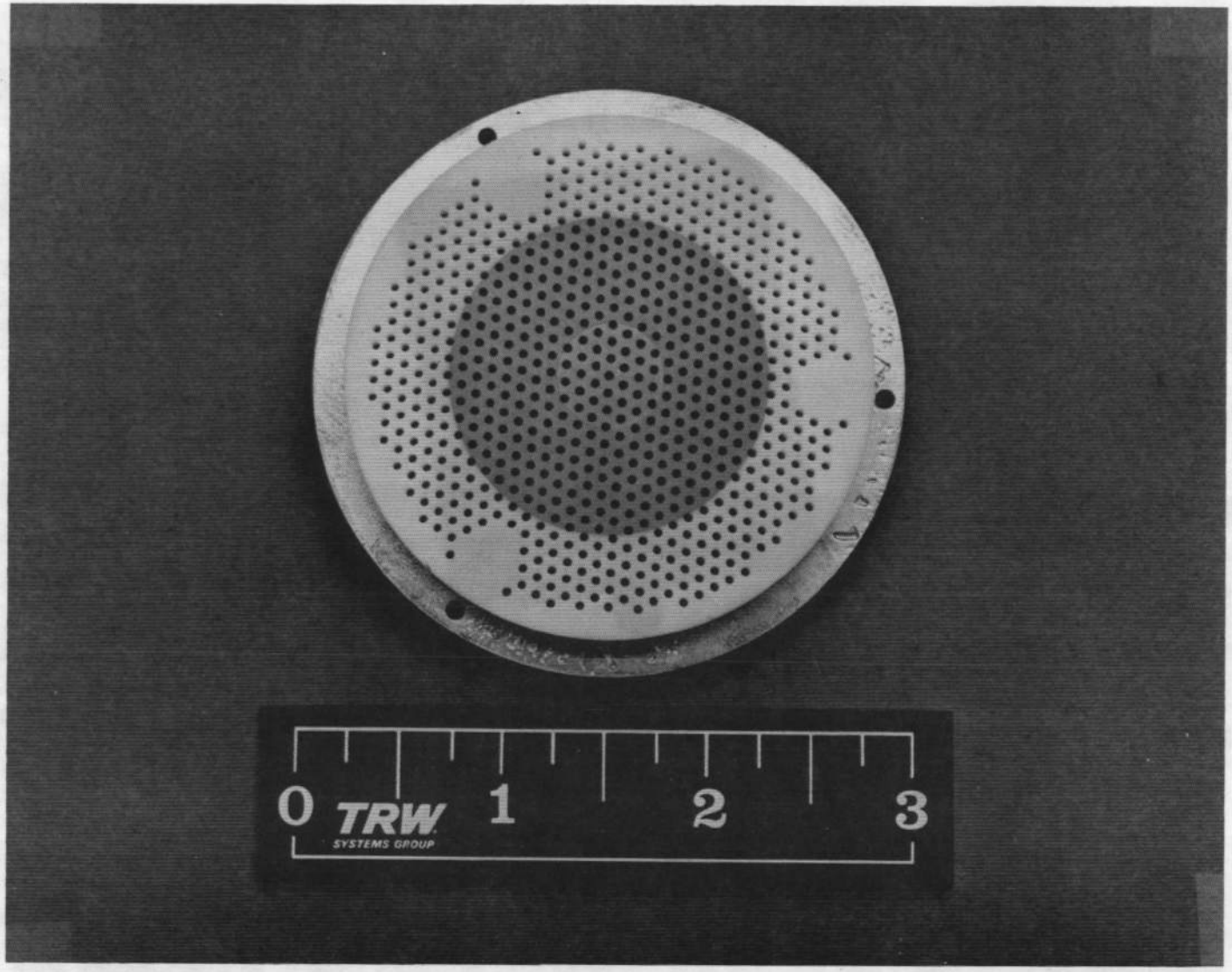

Figure 6. Electrode Assembly

thousand Angstroms thick is deposited for high conductivity. The metallized area shows as the dark area in the center of the electrode plate. Electrical connection is made to the electrode with a leaf spring contact on the opposite side. Connection between the metallized front surface and the back contact surface is made by sputtering gold from both sides in the central 1/2 inch of the electrode plate. This process deposits material on the walls of the holes in this area and establishes good electrical contact. The back side of the electrode assembly can be seen in Figure 7, which is a view of an inside electrode through the common inside volume of the transducer. The central contact metallized area can be seen with the leaf spring connection in contact. The three differential screws used to adjust the electrode spacing (i.e., "fine tune" the capacity) can also be seen. The capacity to the diaphragm of this assembly is approximately 75 pF. The stray capacitance of the arrangement arises almost entirely from the vacuum feedthrough and coaxial connector on the electrode contact and equals 7.5 pF.

3.1.3 Vacuum Materials and Seals

The materials used in the transducer that are exposed to the working volumes all have excellent outgassing characteristics since they are metals (copper, gold, and stainless steel) or glass ceramic. The only organic material exposed to the working volumes is the thin bond line of the polyimide adhesive around the periphery of the diaphragm.

The vacuum integrity of the complete transducer assembly is established by ring seals between the housing pieces and the diaphragm assemblies. In order to maintain vacuum integrity over the objective temperature range, a RACO fluorocarbon-coated "C" ring seal was selected.[6] Unfortunately, considerable trouble was encountered with getting these seals to seat reliably and good vacuum performance was never attained (minimum pressures of about 10^{-4} torr). Therefore these seals were replaced with Viton "O" rings,[7] which are much more limited in their temperature range of operation. Although better vacuum performance was obtained with these seals, they still fell a far short of the objective of 10^{-8} torr. The minimum pressures attained were 5×10^{-7} torr from the common inside volume and 1×10^{-5} torr the parallel combination of the two outside volumes. The poor vacuum performance was determined to be due to leaks rather than outgassing since the vacuum could not be improved by a 24-hour low-temperature bakeout at 80°C and remained stable for two weeks of continuous pumping at room temperature.

3.1.4 Outside and Inside Volume Enclosures

The outside and inside enclosures or housings were also fabricated from OFHC so that the complete transducer was thermally matched. The vacuum connections to these volumes were by stainless steel tubing

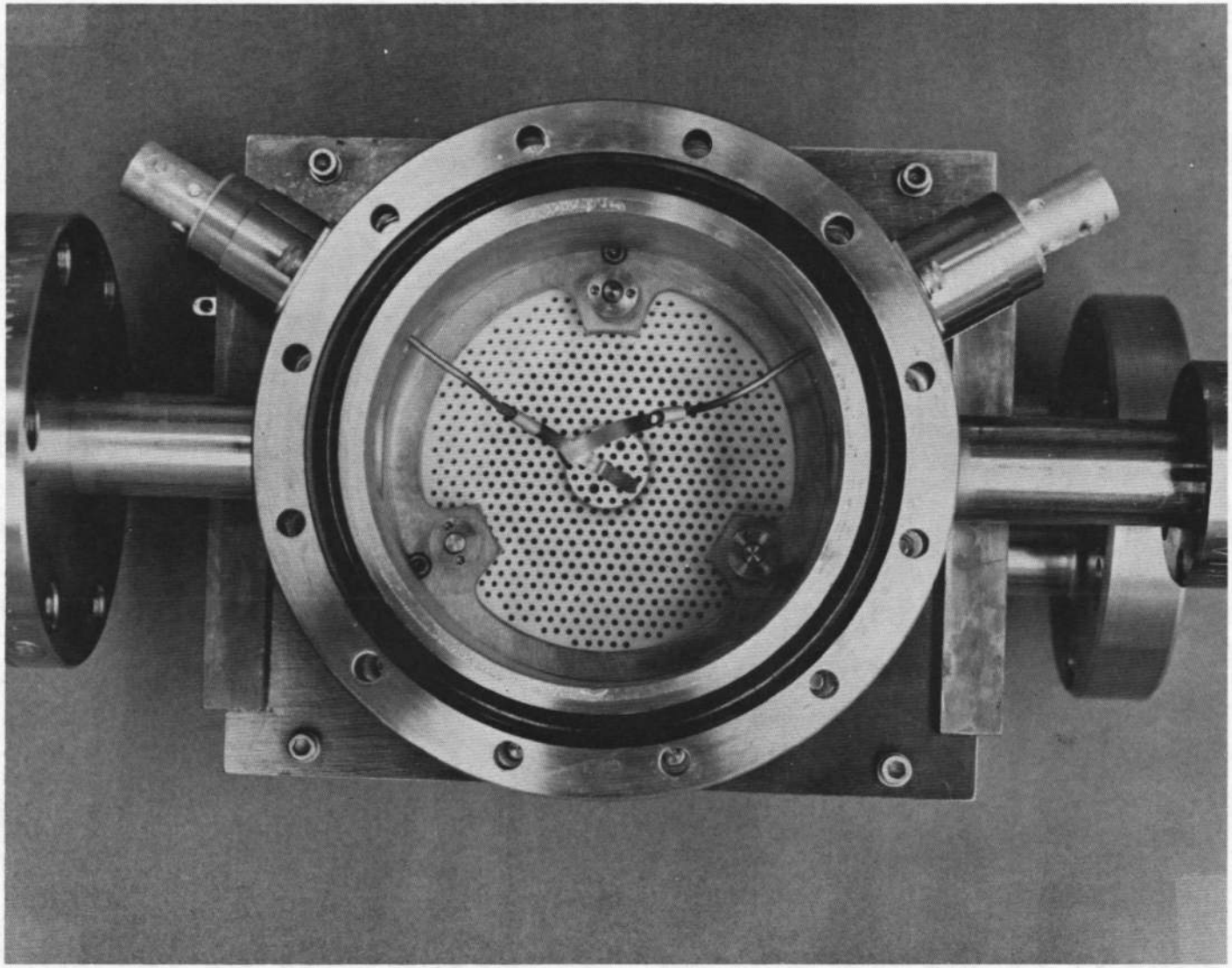

Figure 7. Common Inside Transducer Volume

that was vacuum brazed to the enclosures. Varian Conflat ® copper gasket flanges were used for connections to pumps, etc.[8] The electrical connections through the enclosure walls are vacuum-brazed, metal-ceramic, high-vacuum feedthroughs with shielded coaxial connectors attached on the outside.

3.1.5 Magnet Assembly

As recommended at the conclusion of the previous work, projections were added to the pole pieces in order to maximize the magnetic flux density in the plane of the diaphragm. Although the magnet gap was nominally reduced thereby from the 4 inches of the breadboard transducer to 3.25 inches for the improved transducer, the effect on the magnetic flux density was almost negligible due to the small area of the pole piece extensions. The magnetic fields acting on the diaphragms were measured with a Bell Model 120 gaussmeter. The results are given in Figure 8. They include the proposed iron inserts to concentrate the fields at the diaphragms. The fields tended to increase going away from the membrane center in a vertical direction (toward the poles) and decrease going away from center horizontally (leaving the field). Thus, the $\underline{J} \times \underline{B}$ pressure is not azimuthally uniform (assuming uniform $\underline{J}$), and would tend to excite the m = 2 modes of the diaphragm (two nodes lying on mutually perpendicular diameters). The average field in the central 1.5-inch region is about 640 gauss, and the width of the diaphragm is 3.2 inches for both transducers. Thus, the expected pressure versus current calibration coefficient is from Equation (7):

$$dP/dI = 5.9 \times 10^{-3} \text{ torr/amp.}$$

3.2 ELECTRONICS DESIGN

The main problem was to stabilize a long loop (including the transducer, preamp/modulator, synchronous detector, and diaphragm current drive elctronics) while at the same time maximizing the system sensitivity. A number of modifications were made to the overall loop as described in the report on the previous work.

1) The preamp/modulator was modified.

2) The PAR HR-8 synchronous detector was replaced by a PAR-129A.[9]

3) The Philbrick amplifier/filter was deleted.

4) The diaphragm current driver was redesigned.

The modified loop elements were then combined to form the final system. Because of PAR-129A response limitations, overtones, resonant frequency and Q variation, aliasing, etc., the open-loop response was

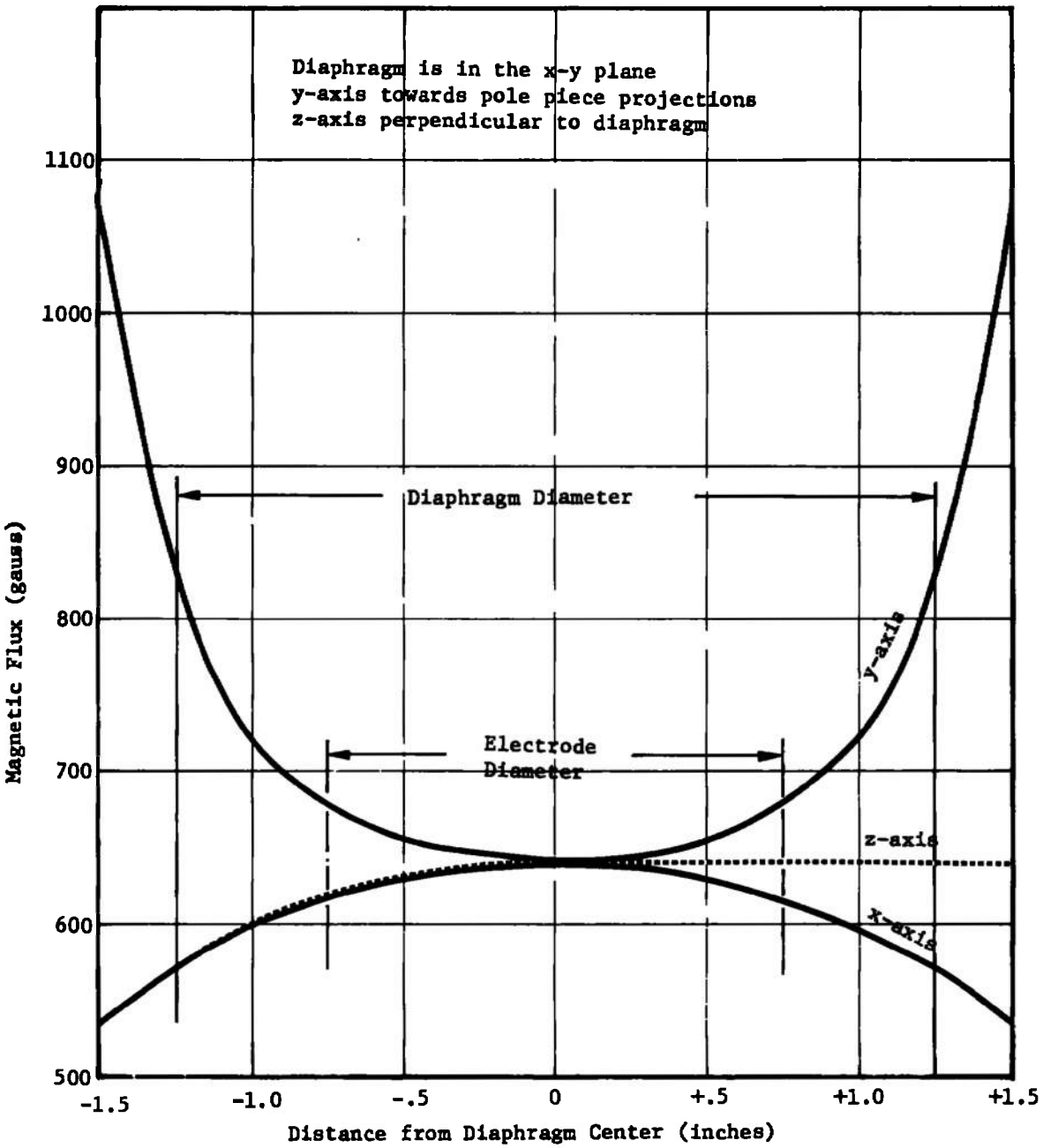

Figure 8. Magnetic Field Characteristics

rolled off early (recall the alternatives discussed in Section 2.2.1). There was thus no feedback damping of the diaphragm vibration pickup; however, such pickup was not a problem at moderate feedback factors (20-40dB).

3.2.1 Design Modification Details

The low-level electronics accumulated two modifications during this contract. First, a specially-balanced drive transformer, T104, provided by MKS Instruments[10] was installed. This modification was made for two reasons. First, the transformer T101, previously used to directly excite the bridge, had considerable capacitive imbalance of its windings. Second, the new transformer allowed us to drive the intermediate shields of the triax cable used to connect to the transducer and thereby remove the effects of cable capacity from the system. This provided the convenience of operating the system with the electronics not constrained to being located right at the transducer.

The LM101A bootstrap circuit, which may be considered as a preamplifier for the weak transducer signal, was modified by removing all compensation and replacing the 101A with the self-compensated uA741. This change eliminated a tendency for self-oscillations in the presence of large bridge unbalance. The modified circuit is unconditionally stable with either one or both of the electrode cables removed causing total bridge unbalance. A LM108 was also tried, but did not have sufficient power bandwidth to drive the cable capacitances at 5 kHz. In addition to the op-amp change, the 22 K balance resistor in the inverting input was bypassed and the feedback capacitor to the bootstrapping point increased to eliminate unnecessary phase shifts.

With the electrode capacitances balanced, the peak quadrature null error at the preamp output (bootstrapping point) is less than 1 mV compared with 10 V at the end of the bridge. This is considered good balance, and the circuit works as well as could be expected. Therefore, no further attempt was made to modify or improve the low level electronics.

The PAR-129A provides simultaneous detection of the inphase and quadrature components of the signal input. The feature was essential for phase-locked loop operation as originally proposed. Phase-locked operation was tried, but it did not yield any advantages that would justify the added complexity. Therefore, the PAR-129A was operated in the simple lock-in mode. The PAR-129A was retained since it made zero adjustments of the bridge very convenient.

With phasing properly adjusted, the zeroing adjustments of the low-level electronics were adequate to set up the system, and were not modified. In addition, the balanced, semifloating ground arrangement of the PAR-129A input was very useful in minimizing the effect of ground loops.

The diaphragm drive stage was extensively modified. Figure 9 is a schematic of the modified circuit. Previously, it included a Philbrick op-amp operated as a low-pass filter, driving an output stage that included a 2N4405 driving a 2N1558 power transistor, both germanium PNP's. The low-pass filter was eliminated in the present work because the PAR-129A output filters provided this function. The Philbrick op-amp was replaced by an LM208. A 0.1-ohm Dale 1% precision resistor was used to sample the diaphragm current. It drove a μA741 differential amp with offset compensation. The output of the diff-amp was returned to the inverting input of the LM208 to provide a single loop encompassing all the drive circuitry. The closed loop rolled off at 12 kHz. The driver amplifier redesign accomplished several objectives:

1) Standardization of output transfer function.

2) Simplification of transfer function by elimination of phase shifts in the frequency range of interest.

3) Linearization of the inherently nonlinear output stage within the driver feedback loop, thus freeing the diaphragm loop from this burden.

4) Virtual elimination of stability and noise feedthrough from diaphragm current power supply.

5) Convenient limiting of diaphragm current at 0 and +10 amperes, using pin-8 clamping on the LM208.

3.2.2 Practical Loop Stabilization

The following procedure was used in setting up and checking the overall loop:

1) Set PAR-129A to "2-phase" mode. Set up preamp and PAR-129A with transducer simulator having two fixed capacitors which simulate the electrode-diaphragm capacitances, plus provision for switch which momentarily adds a small capacitance to one side and subtracts it from the other. Adjust PAR-129 reference phase for maximum response on Inphase meter and minimum on Quadrature meter. Lock the reference phase adjustment.

2) Connect PAR-129 to diaphragm electrodes, and scope to output. With zero pressure differential on diaphragm, balance out the diaphragm capacitance using preamp coarse-balance controls for zero deflection on the corresponding meters, with PAR-129A sensitivity set at middle of its range.

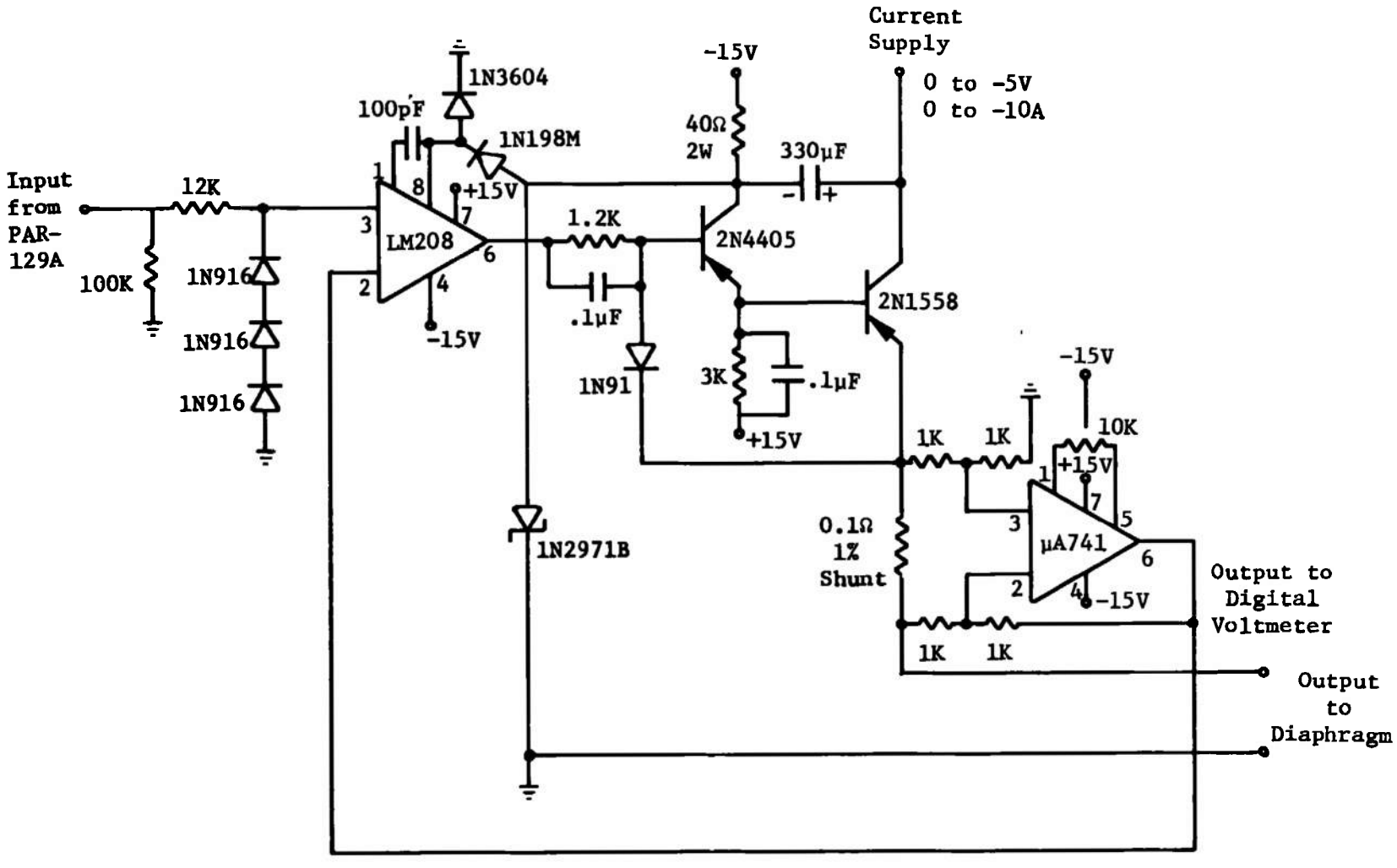

Figure 9. Diaphragm Current-Drive Circuit

3) Excite output driver temporarily with a D.C. supply. With output connected to the diaphragm, the phasing of the J X B pressure may be checked by observing output of PAR-129A connected as discussed above while varying the driver D.C. excitation. The diaphragm connections should be interchanged so that negative feedback will result when overall loop is closed. Note that the diaphragm should be grounded with a 1.0 microfarad capacitor, else there may be noise pickup via the diaphragm connections. At this point, an HP 200CD audio oscillator may also be inserted in series with the driver input, to check frequency response. The driver response across the 100 milohm sampling resistor should be flat up to several kilohertz. With PAR-129A time constant set to minimum, the diaphragm-plus-PAR-129A response should be flat up to the frequency where diaphragm resonance occurs, and will fall off rapidly above that point. With D.C. excitation set to zero, the unipolar driver used in this program delivered half-sinusoids when driven by sinusoids from the HP 200CD. The offset adjustment on the amp was set so that output was exactly zero for positive excursions of input; i.e., on a scope, the "floor" of the signal was set exactly at "ground level".

4) The overall loop is now closed by connecting the PAR-129 output to the driver-input. Increase PAR-129A sensitivity to increase loop gain. Increase time constant to roll off the loop earlier and improve stability. If oscillations occur, open loop by flicking the input selector switch (marked "A/A-B/B") to the ground position until transients quiet down sufficiently to permit loop closure. When the loop is stable, the "overload" light goes out on the PAR-129A, and the output is free from oscillations. The loop feedback factor can be checked by introducing an equivalent differential pressure with the preamp coarse-balance control, then momentarily unplugging the input to the driver. The relative increase in the PAR-129A output is a measure of the feedback factor $(1 + A\beta)$. This factor should be equal to 20 db or more for proper operation.

5) After the loop is properly closed, the various controls can be fine-tuned. When the preamp coarse-balance control is "rocked," the reference phase should be adjusted for zero response on the quad meter. The remaining quad signal can be nulled out with the preamp quad balance control. The inphase meter will indicate the instantaneousl loop error signal.

Loop gain can be increased by turning up the PAR-129A sensitivity control while increasing the time constant to keep the loop stable. At high gains, there is more tendency to overload the PAR-129A input by vibration pick-up in the transducer.

V

SYSTEM TESTS

4.1 TRANSDUCER TESTS

The test setup used to vary and monitor the pressure on each side of the transducer diaphargms is shown in Figure 10. Initial measurements were made to establish the characteristics of the transducer which are critical for closed-loop system operation. These characteristics are the transducer frequency response and the deflection sensitivity.

4.1.1 Frequency Response

In order to measure the frequency response of the transducer, the diaphragms were driven by a variable-frequency sinusoidal source. An HP-200CD variable frequency oscillator coupled with a 30-watt McIntosh audioamplifier delivered a peak current of 4 amperes to the diaphragm. The electrodes were connected in the normal manner to the PAR-129 input. The transfer function of the system, exclusive of the output servo, was thus determined. If the PAR-129 had ideally flat response, the curve would be the transfer function of the transducer with constant-current drive.

The data (Figure 11) show that the diaphragms have a simple displacement-proportional response up to the first diaphragm resonance, and roll off sharply above resonance. There are minor secondary resonances, not shown, around 1 to 1.2 kHz. Diaphragm "Q" is near 500 for pressures up to a few 10's of millitorr, then decreases as the pressure is increased. There is no marked effect of the elastance of the air load on total effective tension. At pressures near 1 atmosphere, some broad "suckouts" were observed at a few hundred Hertz, ascribable to acoustic "organ-pipe" resonances in the vacuum plumbing.

4.1.2 Deflection Sensitivity

The dC/dP of the transducer was directly determined by measuring the electrode-diaphragm capacitance with an ESI-250DA capacitance bridge as the differential pressure across the diaphragm was varied. Figure 12 shows the result of operating the transducer near vacuum and varying the differential pressure across the diaphragm. The two diaphragms have different deflection sensitivities that are correlated with the fundamental resonance frequencies, illustating that the cause of the sensitivity variation is the variation in diaphragm tensioning as expected.

In fact, Table II shows that absolute calculations of diaphragm responses (dC/dP) using Equation (6) are quite close to the experimental values, which verifies the analysis. Thus, for example, diaphragm resonance frequency can be used to study temperature variation of the tensioning and the response coefficient (dC/dP).

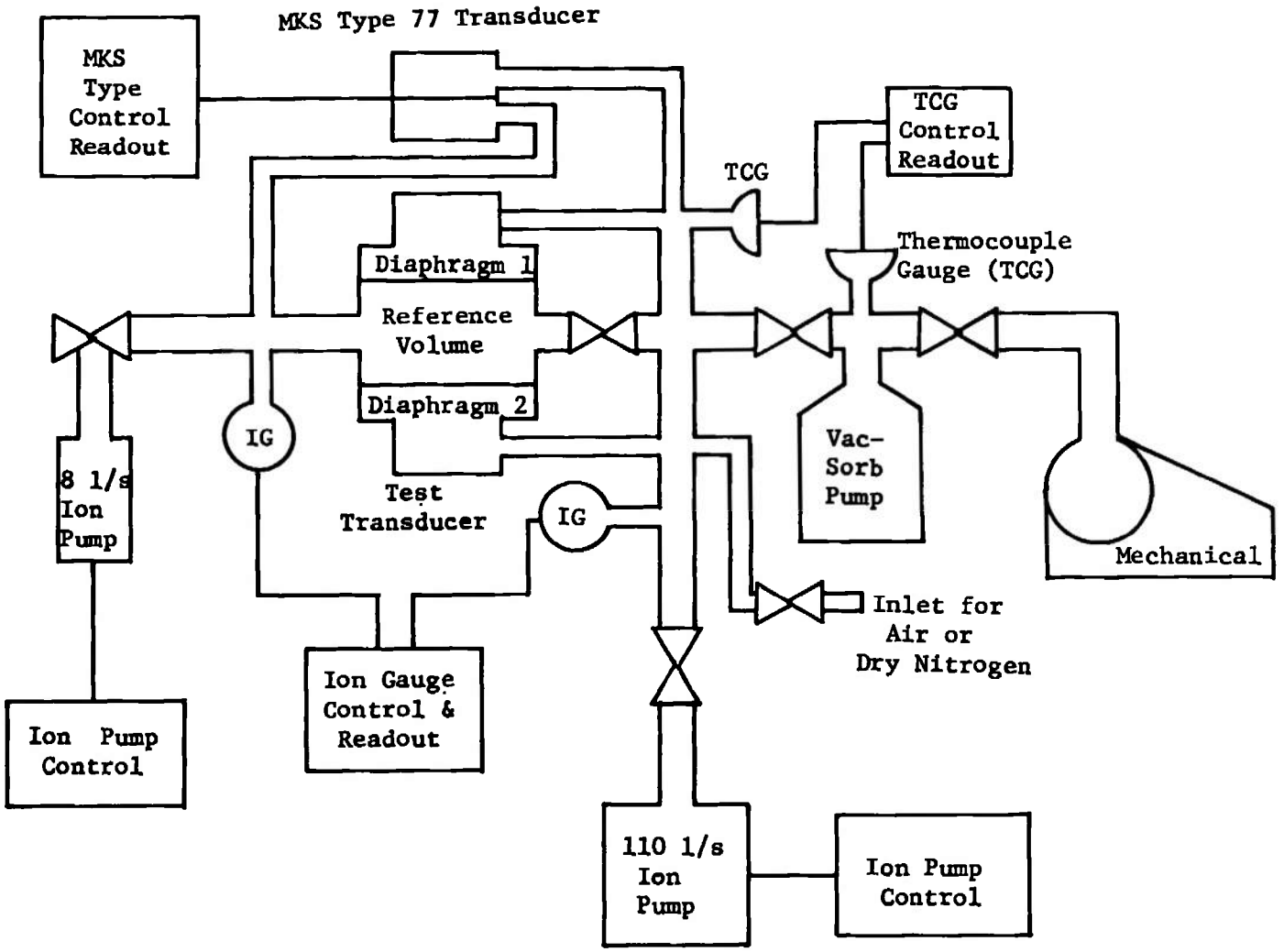

Figure 10. Transducer Test Setup

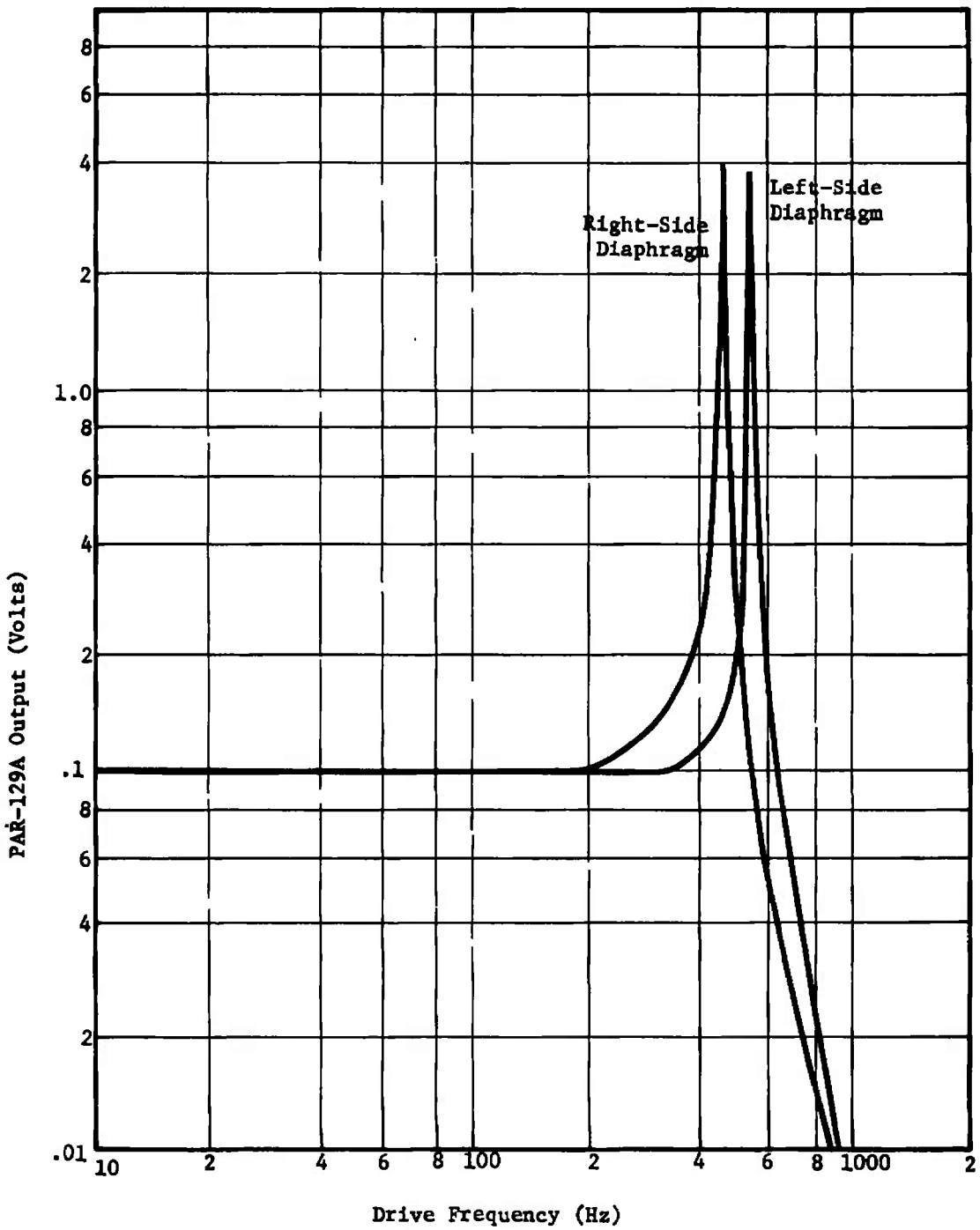

Figure 11. Diaphragm Frequency Response

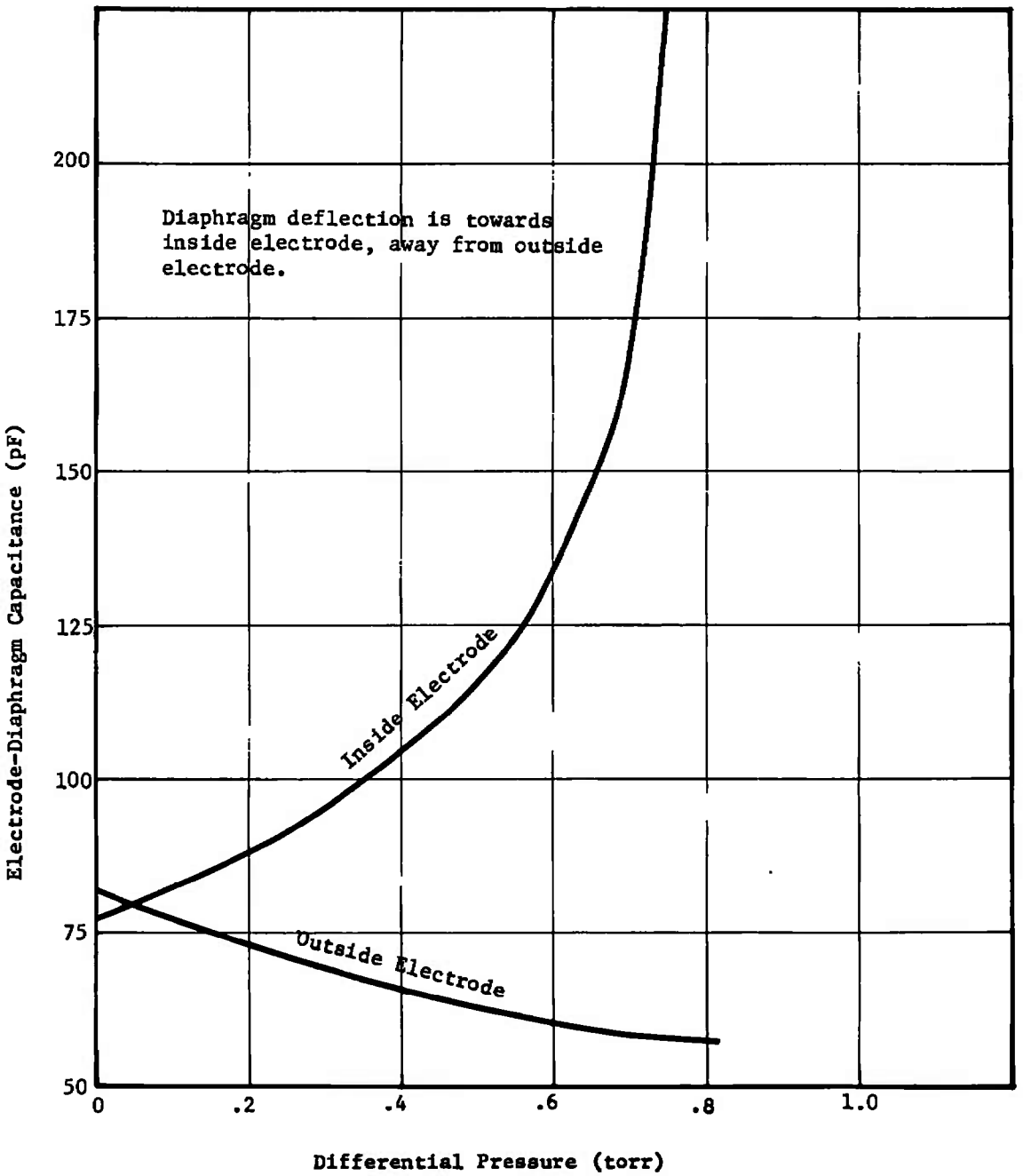

Figure 12. Transducer Deflection Sensitivity

TABLE II

Diaphragm Resonance Frequencies
and Deflection Sensitivities

	Right Side	Left Side
Resonance Frequency (Hz)	461	550
Calculated (pF/torr) dC/dP	45	31
Measure (pF/torr) dC/dP	50	34

4.2 CLOSED-LOOP OPERATION TESTS

The complete closed-loop system, described in Section 3.2, was set up using a Tektronix 545 oscilloscope with 1A7A low-level differential preamp for monitoring the PAR-129A output, and an HP Dymec DVM with 0.1 mV resolution for digital readout. A variable-gain preamp was used at the input to the DVM to adjust the readout calibration factor. Calibration was simplified by the fact that all gains in the diaphragm driver were unity. Thus, 1 mV out of either the PAR-129A or the differential amplifier in the diaphragm driver was equivalent to 1 mV across the 0.1-ohm shunt, or 10 ma through the diaphragm. With the expected pressure-current coefficient of 5.9×10^{-3} torr/amp, the readout calibration would be approximately 1 mV per 6×10^{-5} torr pressure differential. The tests were done using a loop-feedback factor of 20 dB, which was found to be a good compromise. Higher loop gains increased vibration-induced overload and required more time for settling when the loop was opened and closed again, However, it was possible to run at feedback factors as high as 40 dB, and this check was made whenever insufficient loop gain was suspected.

4.2.1 Calibration and Pressure Range

The transducer was operated in a test setup (see Figure 10) that included several types of pressure gauges to monitor the absolute pressure on each side of the diaphragms, and the differential pressure across the diaphragms. The absolute pressure on each side of the diaphragms was measured with calibrated ionization gauges. The absolute pressure of the high-pressure side of the diaphragms was measured with a thermocouple gauge. Finally, the differential pressure across the diaphragms was measured directly by an MKS Baratron, Type 77, Pressure Meter with a 1-torr (full-scale) transducer head.[10]

Figure 13 shows the transducer diaphragm current, as measured by the DVM across the 0.1-ohm shunt in the diaphragm current drive circuit versus the differential pressure indicated by the various

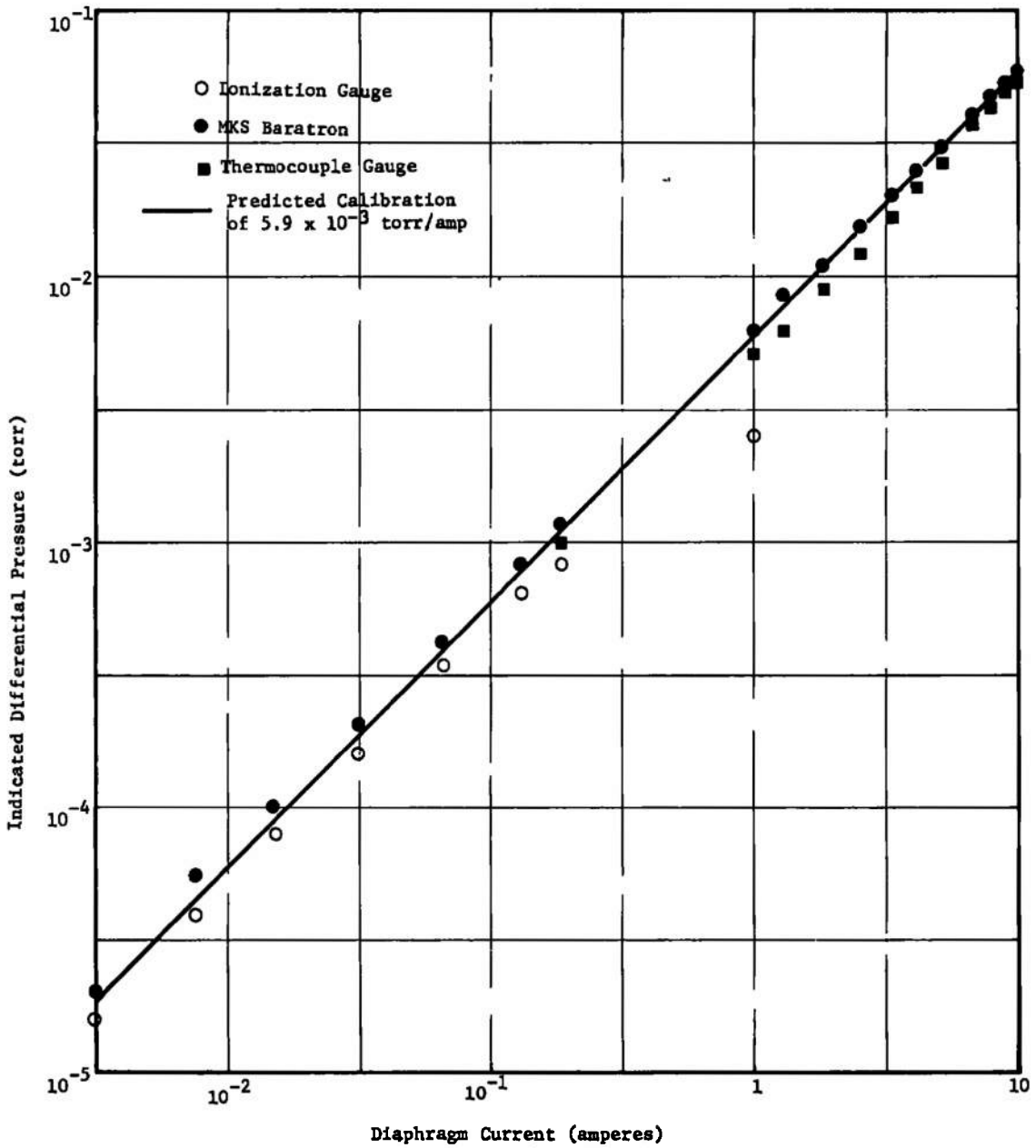

Figure 13. Transducer Calibration Data

reference gauges. We have also plotted the expected calibration curve calculated on the basis of the magnetic field strength (see Section 3.1.5). We can see that the expected calibration falls between the results obtained using the MKS Baratron and the ionization gauges as pressure references. It is impossible to say on the basis of these tests which gauge is most accurate, but the general agreement is good. The upper end of the pressure range was set by the 10-ampere limitation of the diaphragm current supply. Using the calibration above, this limit occurs at about 60 millitorr, which is short of the 100-millitorr objective in the Statement of Work. Although 100 millitorr would require about 16 amperes of diaphragm current, there is no reason that the objective could not be attained with a higher current supply. Calculations analogous to those performed in the previous work[1] indicate that the power dissipation in the diaphragm at 16 amperes is still comfortably below the level that would be expected to completely relax the diaphragm tension. The lower pressure limit at which testing was performed was 10^{-5} torr. The main limitation was leakage of the transducer housing seals. In addition, the necessity of using an offset with the unipolar-type diaphragm driver made it difficult to go lower. Further, there were hysteresis effects, discussed below, which limited repeatability of the zero. However, noise and drift were not limiting factors. 10^{-7} torr-sec^{-1} was the upper bond on drift. Noise was unobservable, and believed to be as calculated elsewhere in this report, near 10^{-8} torr equivalent for 1-Hz closed-loop bandwidth. 60-Hz pickup was equivalent to about 10^{-6} torr, but it is peculiar to the PAR-129A output and could easily be filtered out. Vibration pickup was mostly at the 500-Hz diaphragm resonance, and did not appear in the output (it could easily be filtered if it did). Vibration pickup would not limit attaining 10^{-8} torr; it only affects the attainable feedback factor for reasons partly peculiar to the PAR-129A.

4.2.2 Zero-Shift and Hysteresis

The zero-shift as a function of absolute pressure and relative humidity were investigated in the following manner. The valve between the working volumes on each side of the diaphragms was opened so that no differential pressure across the diaphragm was introduced when the absolute pressure in the system was varied. The absolute pressure was varied from 10^{-5} to 1 torr by introducing either ambient air (approximately 50% relative humidity) or dry nitrogen (approximately 0% relative humidity) into the transducer. The deviations of the diaphragm current were observed during these variations and the results in terms of equivalent differential pressure are shown in Figure 14. Thus while zero-shift was observed, it was relatively small and could easily be adjusted for by rebalancing the bridge circuit with the controls provided.

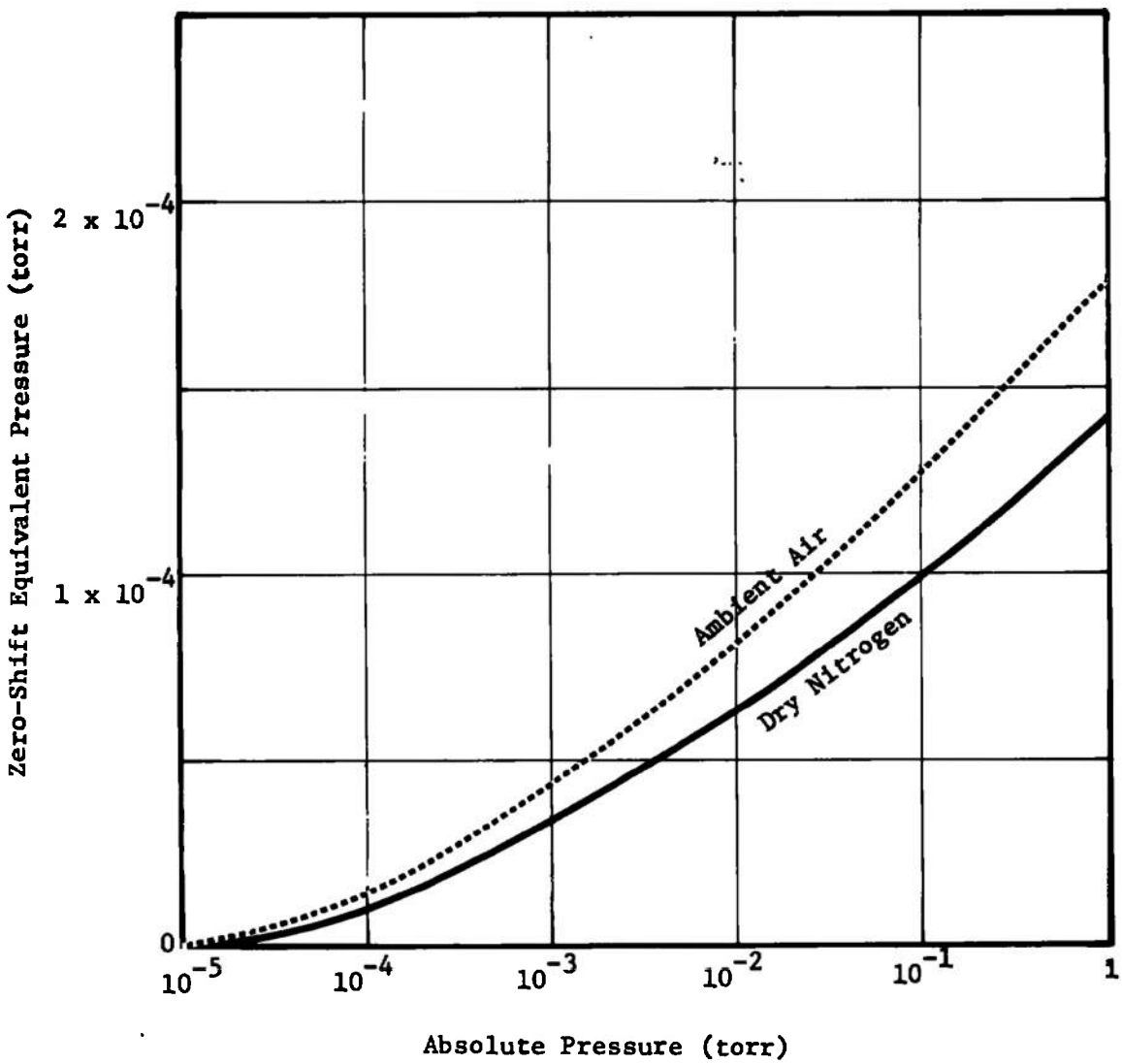

Figure 14. Zero-Shift Characteristics

Hysteresis was observed when differential pressure was cycled up to a high value and then returned to zero. The least hysteresis occurred when the diaphragm movement was reduced by feedback. Cycling to +55 millitorrs and back, with the loop closed, caused about -10^{-5} torrs of hysteresis (i.e., the hysteresis "overshot" in the opposite direction from the pressure transient). The hysteresis would slowly recover with a time constant of about 10 minutes. Increasing loop gain had no effect on this hysteresis.

In the absence of the $\underline{J} \times \underline{B}$ restoring force, e.g., if the diaphragm was deflected in the other direction, or the maximum diaphragm supply current was exceeded, or the loop simply opened up due to a transient; then the hysteresis was sometimes ten times higher.

The amplitude and decay time constant of the observed hysteresis effect was highly variable. They appeared to depend upon both the speed with which the differential pressure excursion was made and the amplitude of the excursion. However, the results were not reproducible except that the direction of the hysteresis was always opposite to the pressure differential. The origin of the hysteresis problem is not understood. For example, it is conceivable that the hysteresis is due to the diaphragm "taking a set" which is then equivalent to a built-in differential pressure offset. If this is the case, higher feedback factor should reduce the effect, which was not observed.

4.3.2 Response Time

The open-loop response time necessary to stabilize the loop with 20 dB feedback was 100 milliseconds, in agreement with the objective in the Statement of Work. When the loop gain was increased to 40 dB it was necessary to increase open-loop response time (PAR-129A output filter) accordingly, but closed-up loop response time was unaffected.

Closed-loop response time was not directly measured, but the system transient response to pressure transients was that expected for 0.1-second response. The measurement could be done by injecting a square-wave current into the diaphragm, at a frequency of about 5 Hz.

The fast system transient response was apparent in the presence on the oscilloscope screen of a "flutter" having an amplitude of a few tens of microvolts. It would be completely eliminated by increasing the PAR-129A output filter time constant by a couple of steps, illustrating the effect of this control on closed-loop time constant.

4.3 TEMPERATURE TESTING

The testing of the transducer performance as a function of temperature was only performed over a range of 20° to 80° C for several reasons. It was not possible to go to higher temperatures because of the Viton "O" rings that were employed to obtain reasonable vacuum integrity. No tests were performed at reduced temperatures because of the lack of suitable facilities to cool the transducer. Finally, and probably most importantly, the behavior of the transducer over even the limited test range indicated that temperature effects were extreme and that there was no hope of stable operation over the objective temperature range. The two most significant temperature effects are discussed below.

4.3.1 Diaphragm Resonance Frequency Change

The diaphragm resonance frequency was measured as a function of temperature using the test setup described in Section 4.1.1. Figure 15 shows the results of one run with the loop open and the PAR-129A frequency response opened up. The resonant frequency and the output amplitude on the plateau below resonance were monitored.

Starting at laboratory temperature of 23°C, the resonance was 405 Hz. (The apparent discrepancy with Figure 11 is due to disassembly and reassembly of the transducer in the interim.) In equilibrium at 55°C, the resonance had moved down to 360 Hz, a 10% drop in frequency implying a 20% drop in tension. This change is also evident in the response, which increased for 15 to 18 mV, or +20%. Since capacitance goes as deflection, and the latter goes inversely as tension, the effect is as expected. The origin of the tension change is presumably thermal mismatches in the transducer.

The principal effect of the change in diaphragm resonance frequency is to very the stability of the feedback loop. As the resonance frequency moves down towards the unity-gain point of the closed loop, the system will become increasingly prone to break into oscillation due to acoustic vibrations of the transducer.

4.3.2 Capacitance Changes

As was discussed in Section 3.1.2, the transducer electrode assemblies were designed to have identical behavior as a function of temperature and, hence, to cancel any first order temperature effects on transducer operation. The initial tests on the temperature sensitivity of the transducer showed a very large drift in the system output equivalent to approximately 2×10^{-4} torr/°C. In order to determine the origin of this effect, the capacitances between each of the electrodes and their respective diaphragms were measured as a function of temperature. The results are shown in

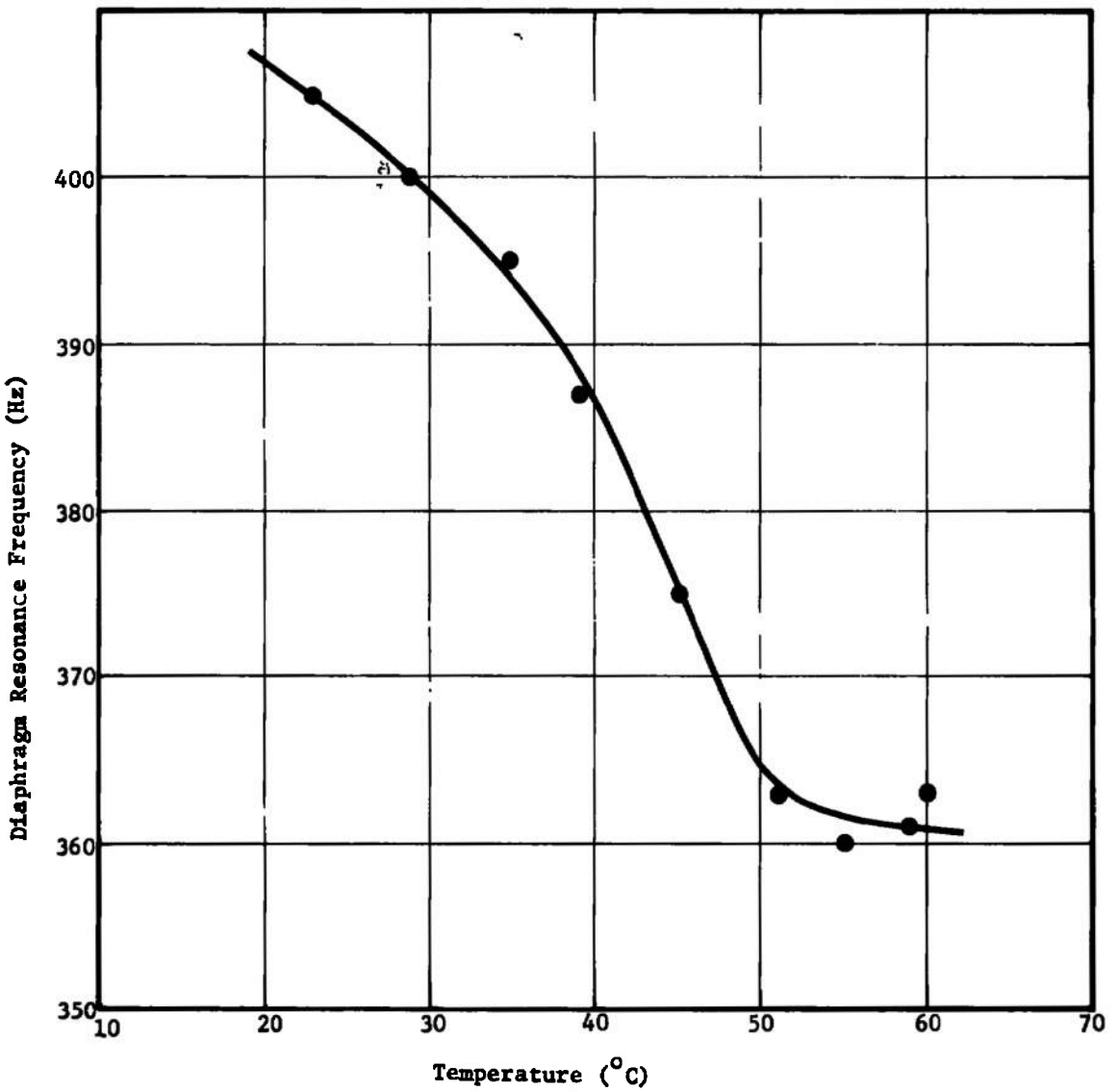

Figure 15. Temperature Dependence of Diaphragm Resonance Frequency

Figure 16. It is apparent that the capacitances are not changing equally as the temperature is varied and, hence, the null point is also varying. The magnitude of capacitance change versus temperature completely accounts for the drift given above. We believe the cause of the nonidentical behavior of the individual electrodes lies in small differences in the electrodes as assembled and thermal coefficient mismatches in the electrode mounting arrangements. In any case, it does not appear to be feasible to achieve the match in electrode characteristics required for stable operation as a function of temperature. In the present transducer design, the electrode to diaphragm spacing changes at a rate of about 4×10^{-6} inches/°C due to differences in the thermal expansion coefficients of copper and the glass-ceramic electrode material. This corresponds to a change of capacitance of approximately 0.1 pF/°C, which is equivalent to about 2×10^{-3} torr/°C. A temperature drift compatible with the transducer-limiting sensitivity of 10^{-7} torr/°C would require electrode movement that was matched to 1 part in 10^{-4} and the absence of temperature differentials greater than the order of 10^{-4} °C in the electrode-diaphragm assembly.

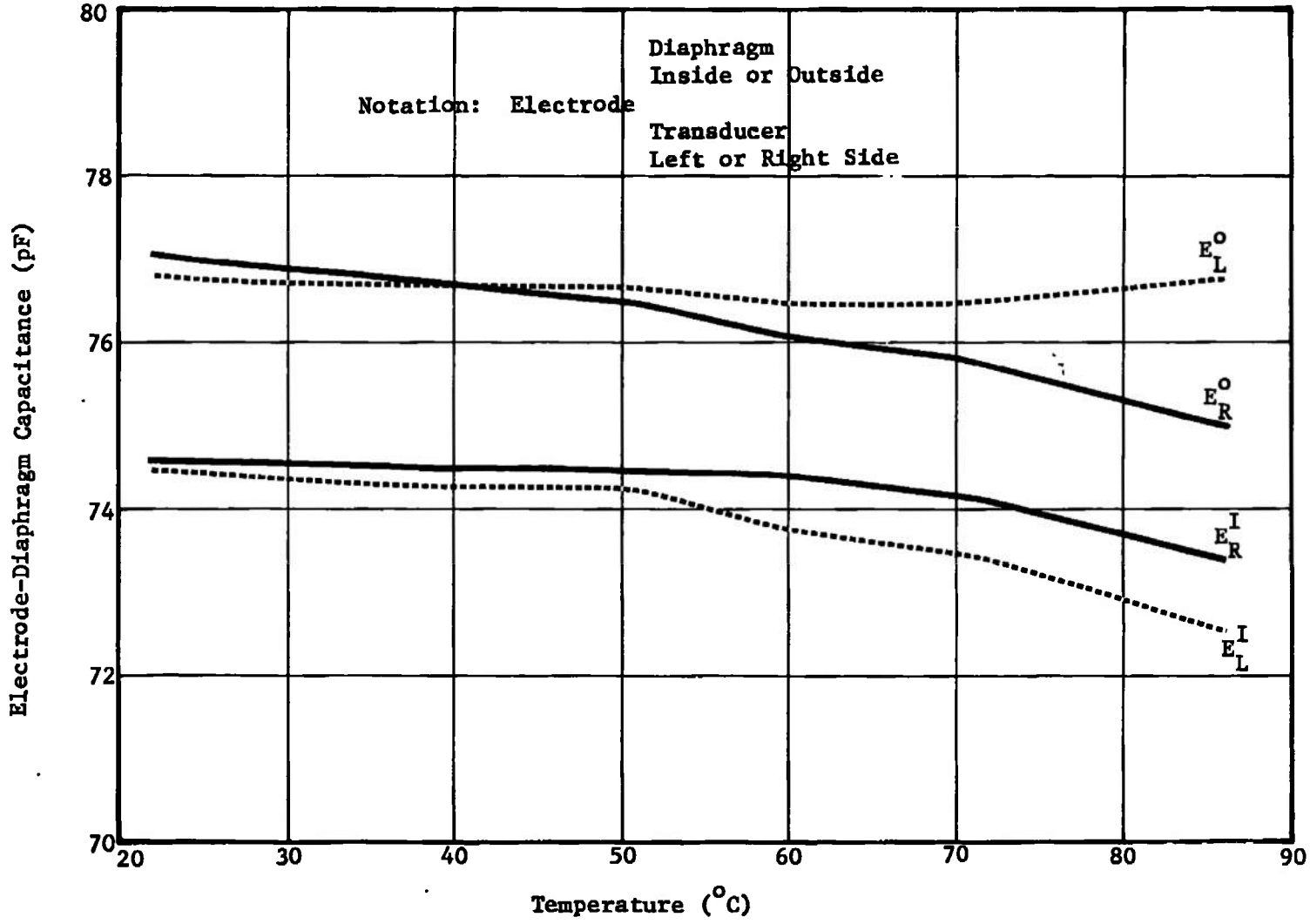

Figure 16. Temperature Dependence of Transducer Capacitances

V

CONCLUSIONS

5.1 IMPROVED TRANSDUCER PERFORMANCE

In summary, the improved transducer developed in the present work had the following performance characteristics:

1) Operation was demonstrated in the pressure range of 6×10^{-2} to 1×10^{-5} torr. The upper end of the pressure range was set by the 10 amperes maximum current at the diaphragm current drive circuit used and is not at all fundamental. Extension to 1×10^{-1} torr could be achieved with simple modification of the drive circuit and power supply. The lower end of the pressure range was set primarily by the vacuum performance of the transducer. Again, this is not a fundamental limitation of the transducer. Better vacuum performance should be attainable with design modifications. The limit of the present transducer system for practical operation is expected to be 1×10^{-6} torr if the response speed is maintained at 100 milliseconds. A limit of 1×10^{-8} torr is theoretically attainable at the sacrifice of response time, but the system would be extremely sensitive to vibrational overload at the diaphragm resonance frequency. Operation would be extremely touchy and probably not really useful in practice.

2) The severe difficulties encountered with transducer operation in the limited temperature range of 20 to 80°C convinced us that operation over the objective temperature range of -268 to +250°C is completely unpracticable. The materials problems involved in maintaining transducer vacuum integrity over that temperature range may be soluble, but not without extensive development and testing. Operation should be possible over a more modest temperature range (e.g., -100 to ±100°C) if the transducer was temperature controlled to essentially remove all temperature gradients in the internal structure.

3) The use of low water-absorbing materials in the improved transducer achieved the desired characteristic of minimal sensitivity to humidity. The effect on zero shift was easily adjusted for with the available balance controls.

4) The measured drift of the transducer null with temperature was equivalent to a pressure calibration zero drift of 2×10^{-4} torr/°C. This excessive drift made measurement of the calibration constant dP/dI as a function of temperature impossible because the measurement would have to be made at a constant temperature. This required that the heaters be on which produced large 60 cycle pick up on the electrodes and made sensitive measurements impossible.

5) The excessive zero shift as a function of absolute pressure experienced in the previous work was largely eliminated in the improved transducer. That which was observed was well within the range of easy adjustment and was reproducible. However, a hysteresis effect was discovered. When the differential pressure was varied through a cycle starting at zero and returning to zero, the transducer output returned to a negative value. This offset decayed to zero with a typical time constant of about ten minutes. The magnitude of the hysteresis was sensitive to the speed and amplitude of the pressure cycle but not in a reproducible manner. A typical best case (i.e., slow pressure excursion within the operational range of 0 to 6×10^{-2} torr) value of the hysteresis was -1×10^{-5} torr. The cause of this effect was not determined in the present work.

6) Although the response time of the transducer was not directly measured, the value derived from the measured frequency response of the electronic closed-loop feedback system was equal to the objective of 100 milliseconds when a feedback factor of 20 dB was used. This feedback factor was the value at which maximum practical transducer sensitivity would be 1×10^{-6} torr. Greater sensitivity would require a corresponding reduction in response time.

5.2 RECOMMENDED DESIGN IMPROVEMENTS

There are several areas in which improvements to the present transducer design are believed possible. In several cases these improvements are straightforward to implement. These include:

1) Elimination of the parallel diaphragm design because a dual diaphragm transducer has no advantage over single diaphragm design which would be simpler and cheaper to produce.

2) Incorporation of a recently available bipolar operational power supply[11] in place of the current drive circuitry. This new unit is more flexible and would offer convenient operation for positive and negative differential pressures.

3) Optimization of the magnet configuration to increase the field and make it more uniform. This would require replacement of the present off-the-shelf magnet assembly with a custom designed and fabricated unit. It should be possible to double the useful magnetic field.

Two other areas of design improvement would require considerable development to arrive at signficant improvements. These are:

4) Development of an improved housing seal for high vacuum performance. Some type of metal-to-metal seal is probably required. The alternatives would be replaceable seals such as a metal "O" ring or permanent metal bonding of the assembly. In either case, the transducer would not be easily disassembled in the field.

5) Development of improved diaphragm bonding adhesives and techniques. Although the present diaphragm bonding concept is felt to be basically sound considerable improvement and/or increased reliability and reproducibility should be possible with further work on adhesive material selection and bonding process control.

REFERENCES

1. Research and Development of a Pressure Transducer for Test Chamber Measurement, O. O. Fiet, TRW Systems Group, Report No. AEDC-TR-71-144, 1971.

2. An Improved Ultra Sensitive Pressure Meter for Test Chamber Measurements, TRW Systems Group, Proposal No. 21263.000, 1971.

3. Vibration and Sound, Morse, McGraw-Hill Book Co., 1948.

4. Kerimid 500, Rhodia Inc., 600 Madison Ave., New York, N. Y. 10022.

5. Machinable Glass-Ceramic, Corning Glass Works, Corning, N. Y. 14830.

6. Raco Seal No. 1171-3.005-9-0, The Fluorocarbon Co., 22624 Avalon Blvd., Carson, Calif. 90745.

7. Viton O-Ring, Parker Seal Co., 10567 Jefferson Blvd., Culver City, Calif. 90230.

8. Conflat Flange, Vacuum Division, Varian Associates, 611 Hansen Way, Palo Alto, Calif. 94303.

9. Two Phase/Vector Lock-In Amplifier, Model 129A, Princeton Applied Research, P. O. Box 2565, Princeton, N. J. 08540.

10. MKS Instruments, Inc., 25 Adams St., Burlington, Mass. 01803.

11. Bipolar Operational Power Supply/Amplifier (±15 volt output rated at ±20 amperes), Kepco, Inc., 131-38 Sanford Ave., Flushing, N. Y. 11352.